Joint evolution of irrigation, the water cycle and water resources under a strong climate change scenario from 1950 to 2100 in the IPSL-CM6

Pedro Felipe Arboleda-Obando[1,2], Agnès Ducharne[1,2], Frédérique Cheruy[2,3], Josefine Ghattas[2]

[1] Laboratoire METIS (UMR 7619, Sorbonne Université, CNRS, EPHE), Paris, France
[2] Institut Pierre Simon Laplace (FR 636, Sorbonne Université, CNRS), Paris, France
[3] Laboratoire de Méteorologie Dynamique (UMR 8539, Sorbonne Université, CNRS), Paris, France

Corresponding author: Pedro Felipe Arboleda-Obando (pedro-felipe.arboleda-obendo@univ-grenoble-alpes.fr)

Abstract. Irrigation, a key activity for food security, uses local water resources to increase evapotranspiration, creating feedback loops with the atmosphere and water resources. With climate change, it is unclear how irrigation will evolve in the future and how it may influence the evolution of water resources and the water cycle. It is also unclear whether irrigation may be constrained by climate change or water resource shortages. Here, we compare two surface–atmosphere simulations performed with the IPSL-CM6 model from 1950-2100: one with irrigation and one without irrigation. In both simulations, the evolutions of atmospheric radiative forcing, land use, and irrigated areas are taken from CMIP6, which uses a historical dataset for the data before 2014 and the SSP5-RCP8.5 dataset for data after 2014. The two simulations reveal strong global warming and precipitation increases between 1950-2000 and 2050-2100 average values (+5.6 °C and +8.1%, on average, over land with irrigation). Over the same period, our results indicate an increase in irrigation (+76% increase in irrigation in the 2050–2100 compared to the 1950–2000 period), which is in line with a significant expansion of irrigated areas. The influence of irrigation on evapotranspiration in irrigated areas is greater in 2050-2100 than in 1950–2000 (+12% vs. +8%, respectively). Evapotranspiration has also been found to increase in non-irrigated areas near irrigated zones owing to an increase in precipitation under historical and future climate conditions. Water depletion due to irrigation is more intense in the future than in the historical period, although climate change increases water storages and river discharge due to more precipitation in the future. We also identified areas where future environmental conditions can limit irrigation or where irrigation can increase tensions over water use (approximately one-third of irrigated areas, including the Mediterranean basin, California, and Southeast Asia). Our results highlight the importance of considering irrigation in climate projections and future water resources assessments.

1 Introduction

Irrigation supports approximately 43% of the world's production on approximately 20% of arable land (Grafton et al., 2017; Siebert and Döll, 2010). As a direct consequence, 70% of human water withdrawal is used for irrigation (between 2657 and 3594 km³ y⁻¹ in 2000, Pokhrel et al. (2016a)). The key role that irrigation plays today in food production and the corresponding water demand is the result of a significant increase in the irrigated area during the 20th century (a fivefold increase between 1900 and 2005, Siebert et al. (2015a)). This expansion of irrigation may continue in the future, as the replacement of rainfed cropping systems with irrigated systems is one of the measures used to adapt agriculture to climate change (Okada et al., 2018). In addition to its beneficial effects on food production, irrigation has a direct effect on water and energy balances and surface and subsurface hydrology (Döll et al., 2012; Taylor et al., 2013). Such effects can even drive the evolution of certain variables over time (Al-Yaari et al., 2022; Vicente-Serrano et al., 2019). In addition, the increase in evapotranspiration (ET, due to increased crop transpiration and higher near-surface soil moisture) also induces atmospheric feedback loops such as air temperature cooling (Thiery et al., 2020) and changes in precipitation patterns at different scales that affect the water cycle (Al-Yaari et al., 2019; Cook et al., 2015; Guimberteau et al., 2012b; Lo and Famiglietti, 2013; de Rosnay et al., 2003; de Vrese et al., 2016a).

With the acceleration of climate change, there are concerns related to the future of irrigation, as well as its effects on water resources under a changing climate. This has led to global projections (Wada et al., 2013a; Khan et al., 2023a) via global hydrology models (GHMs). However, these modeling efforts with GHMs prescribe atmospheric forcing, so the interaction between irrigation and the atmosphere is not considered.

To consider joint projections for water resources, irrigation, and climate, irrigation must be represented in land surface models (LSMs) within Earth System Models (ESMs), and the LSM must be run in coupled mode with an atmospheric model (McDermid et al., 2023). In recent years, many LSMs have included irrigation modules, such as ORCHIDEE (Yin et al., 2020; Arboleda-Obando et al., 2024a), CLM (Leng et al., 2013; Yao et al., 2022), ISBA-SURFEX (Druel et al., 2022), and MIROC (Pokhrel et al., 2012, 2015). While some of these LSMs have been used in coupled mode under a historical climate (see Al-Yaari et al. (2022a)), coupled simulations under a future climate scenario are less common (Cook et al., 2020). This means that the coupled evolution of irrigation activities, water resources, and climate under a future climate change scenario needs to be further explored.

Here, we present the results of a pair of coupled simulations using the Institut Pierre Simon Laplace Climate Model 6 (IPSL-CM6), the version used for the Coupled Model Intercomparison Project phase 6 (CMIP6). In Section 2, we present the atmospheric and land surface components of the IPSL-CM6, including the main characteristics of the irrigation scheme; then, we present the modeling setup and analysis methods. In Section 3, we explore how irrigation rates are expected to evolve from 1950-2100. We then evaluate the evolution of the influence of irrigation on variables related to the water cycle and water resources. We also explore the limits to irrigation growth under future hydroclimate conditions to identify areas where tensions over water use might increase due to irrigation or where irrigation expansion could be possible. Finally, we discuss the

61 limitations of our results and their implications for climate projections and water resources assessments under future climate
62 conditions.

63

64 **2 Methodology**

65 **2.1 LMDZOR model**

66 We used the LMDZOR model (Cheruy et al., 2020), which involves the coupling of the atmosphere and land components of
67 the IPSL-CM, respectively the LMDZ (Laboratoire de Météorologie Dynamique with Zoom capacity) and ORCHIDEE
68 (Organising Carbon and Hydrology In Dynamic Ecosystems) models. ~~We briefly describe each component.~~ This version uses
69 the LMDZ6A atmospheric model (Hourdin et al., 2020; Sadourny and Laval, 1984) embedded in IPSL-CM6A-LR (Boucher
70 et al., 2020), but we used a medium resolution rather than the standard low resolution (MR and LR, respectively), i.e., 256x256
71 grid cells, approximately 1.41°x0.71° in size, and 79 vertical levels. Except for the resolution, the configuration remains close
72 to the model used for CMIP6.
73 The LMDZ model uses a finite difference discretization of the primitive meteorology equation on an Arakawa C grid, favoring
74 the conservation of entropy rather than that of energy (Boucher et al., 2020). It can refine the grid in both longitude and latitude,
75 and the Z in LMDZ indicates its zoom capabilities. Apart from the dynamics, the model couples physical parameterizations of
76 different processes through a generic interface that computes the vertical transfer of those physical processes. The LMDZ6A
77 version includes important improvements in several processes: it computes eddy diffusion by introducing prognostic turbulent
78 kinetic energy (TKE), with particular attention given to the representation of very stable boundary layers over ice sheet plateaus
79 and boreal lands. It also includes a boundary layer convection module, represented by a thermal plume model, with a time
80 implicit scheme and upwind space finite volume scheme for numerical stability and a better representation of stratocumulus
81 clouds. Finally, it also includes a new deep convection module that assumes coupling between shallow convection and deep
82 convection at the cumulus base level, with a statistical estimate of the maximum vertical velocity (Hourdin et al., 2020).
83 The O~~rganising Carbon and Hydrology In Dynamic Ecosystems,~~ ORCHIDEE land surface model describes the mass,
84 momentum, and heat fluxes between the surface and the atmosphere (Krinner et al., 2005). The version used here corresponds
85 to ORCHIDEE 2.2, which is similar to the ORCHIDEE 2.0 model used in CMIP6 (Boucher et al., 2020; Cheruy et al., 2020)
86 but includes some minor bug corrections and a global irrigation scheme that was recently developed and evaluated (Arboleda-
87 Obando et al., 2024). The soil column was set to a depth of 2 m, but we used a version with 22 layers instead of 11 layers, so
88 the soil humidity in the root zone defined for the irrigation scheme was finely modeled. ORCHIDEE has been extensively
89 described elsewhere, and we summarize here the main characteristics of the model.
90 The turbulent fluxes between the surface and atmosphere use the Monin–Obukhov theory and the bulk formulations proposed
91 by Louis et al. (1982). However, the stability functions for the calculations of the surface drag coefficients proposed Louis et

92 al. (1982) are replaced by functions proposed by (King et al., 2001) to better represent stable conditions (Vignon et al., 2017).

93 Additionally, the computation of the surface roughness height has been improved by introducing a dynamic roughness height.

94 Vegetation is represented by 15 plant functional types (PFTs, including bare soil), each with different parameter values to

95 simulate photosynthesis and carbon allocation; carbon fluxes and plant phenology are controlled by the STOMATE (Saclay

96 Toulouse Orsay Model for the Analysis of Terrestrial Ecosystems; Krinner et al. 2005) module, which computes the evolution

97 of the leaf area index (LAI) . Note that no specific crop phenology module was used, following Arboleda-Obando et al. (2024),

98 owing to a lack of ubiquitous parameters at the global scale. It means that C3 and C4 crops are assumed to have the same

99 phenology as natural grasslands but with higher carboxylation rates. Remark that this simplification may have an impact on

100 the timing and volume of total water withdrawal, by inducing an overestimation of water demand and ultimately water use (if

101 there is available water offer; Arboleda-Obando et al. 2024). This is due to the lack of representation of the crop calendar,

102 including the harvest stage, which keeps the leaf area index values high in the model.

103 Evapotranspiration follows a classical bulk aerodynamic approach with four subfluxes: snow sublimation, interception loss,

104 bare soil evaporation and transpiration. There are three soil tiles according to vegetation type (bare soil, forest, and crops and

105 grasses) within each grid cell. Surface infiltration is represented as a sharp wetting front based on the Green and Ampt model,

106 whereas vertical soil flow is represented by a 1-D Richards equation (D'Orgeval et al., 2008; Tafasca et al., 2020). The soil is

107 assumed to be homogenous inside the grid cell and is represented by the dominant USDA soil texture according to the map

108 from Zobler (1986). While lateral fluxes between grid cells are neglected, a routing scheme transfers surface runoff and

109 drainage from land to the ocean through a cascade of linear reservoirs (Guimberteau et al., 2012a; Ngo-Duc et al., 2007). Each

110 grid cell is split into transfer units (also called subbasins) with the river reservoir and two local reservoirs: overland and

111 groundwater. Subbasins are defined according to a flow direction map from Vörösmarty et al. (2000) and are enhanced over

112 the polar region by Oki et al. (1999). Note that owing to the coarse resolution, it is possible to have more than one transfer unit

113 inside every grid cell.

114 While the water balance is independent for each soil tile, the energy balance is the same for the whole grid cell. The surface

115 energy and water budget computation time are the same as that of the atmospheric model, which is 15 minutes. The routing

116 scheme also uses a 15-minute time step (the standard is one day) to finely follow changes in reservoirs due to water withdrawal.

117 In contrast, the carbon and plant phenology computed by STOMATE uses a daily time step.

118 **2.2 Irrigation scheme**

119 The irrigation scheme used here was tested and evaluated in Arboleda-Obando et al. (2024a) at the global scale. This work

120 included a sensitivity analysis to understand the effect of each parameter on irrigation volume and evaporation increase, leading

121 to choosing a set of globally homogenous parameters enabling a good match between simulated and reported values of global

122 irrigation withdrawal. Here, we briefly describe its main characteristics. First, the root zone depth is set according to a user-

123 defined parameter. In our case, we set this depth to 0.65 m (11 layers). This depth comprises approximately 90% of the crop

124 root system as represented in ORCHIDEE. Then, at each time step, the scheme calculates a soil moisture deficit. This deficit

125 is the difference between the actual soil moisture and a user-defined target in all the root zone layers. We set this target to 0.9

126 times the soil moisture at field capacity. Third, we calculate the irrigation requirement using the prescribed fraction of irrigated

127 grid cells and limit the maximum irrigation per hour to 3 mm/h.

128 In the fourth step, the module estimates the available water in the natural reservoirs (overland, groundwater, and river

129 reservoirs), with two constraints: a factor to prevent total depletion of the natural reservoir and mimic an environmental flow

130 (set to 0.9 for all three reservoirs) and the facility for accessing the natural reservoir as represented by a prescribed map of

131 irrigated areas that are equipped for surface or groundwater use (Siebert et al., 2010). The facility of water access helps to

132 prioritize one reservoir over others; for instance, in a gridcell with irrigation demand and groundwater availability but no

133 groundwater access infrastructure, all the water supply will come from the surface reservoirs (overland and stream). More

134 details can be found in Arboleda-Obando et al. (2024). Apart from the local reservoirs, the scheme allows river water adduction

135 from local transfer units (also called subgrid basins in Ngo-Duc et al. 2007) within the grid cell, limiting the available water

136 with a factor set here to 0.05 to prevent river depletion. Owing to the coarse scale, water adduction from neighboring grid cells

137 is deactivated.

138 In the final step, the scheme estimates the maximum water requirement and water supply (locally available water and

139 adduction) and withdraws the volume from the natural reservoirs. The withdrawn water is added at the soil surface for

140 infiltration, thus resembling a flood or drip irrigation technique. This implies that not all of the water volume is involved in

141 transpiration or bare soil evaporation, as the model decides if part of this volume becomes surface runoff or groundwater

142 recharge. The scheme does not represent paddy rice as a different irrigation technique and uses global homogenous parameters

143 taken from Arboleda-Obando et al. (2024a).

144 We note here some shortcomings identified in the irrigation scheme used here (Arboleda-Obando et al., 2024). The scheme

145 represents a single irrigation technique (the flood technique), and uses a set of simplified rules to trigger irrigation and allocate

146 available water. Besides, the scheme uses a joint representation of rainfed and irrigated crops within the same tile, and the

147 scheme doesn't represent conveyance losses. To restrain in part the effect of these shortcomings on estimated irrigation

148 volumes, parameter values were tuned by fitting the simulation to reported irrigation datasets. But we must also note that this

149 parameter tuning is overly simplistic, as it uses globally uniform parameters. Despite these limitations the irrigation scheme

150 produces acceptable estimates of yearly estimation withdrawals at global scale, but tends to underestimate irrigation

151 withdrawals in China, India and the USA, corresponding to the irrigation hotspots (Arboleda-Obando et al., 2024).

152 **2.3 Radiative forcing and socioeconomic scenario**

153 We ran two simulations, one without the irrigation scheme (NoIrr simulation) and a second with the irrigation scheme activated

154 (Irr simulation), for the period 1950 to 2100. Each simulation runs 50 years of spin-up with a prescribed sea surface

155 temperature/sea ice content (SST/SIC) from the AMIP dataset and historical radiative forcing.

156 The radiative forcing is prescribed using historical (1950-2014) and SSP5-RCP8.5 (2015-2100) datasets from ScenarioMIP

157 (Tebaldi et al., 2021). The use of scenario SSP5-RCP8.5 could be seen as the upper boundary of potential climate change

158 impacts and results in a strong global warming and important changes in precipitation. The use of this scenario allows for
159 analysis of the interaction between irrigation and climate in a context of strong climate change signals and significant changes
160 in irrigated land area. For oceanic conditions, the simulations were run with a prescribed bias and variance-corrected SST/SIC
161 dataset (Beaumet et al., 2019) constructed on the basis of the SST/SIC simulated by the fully coupled IPSL-CM6 and observed
162 AMIP. This fully coupled simulation uses historical and SSP5-RCP8.5 data to prescribe radiative forcing as well. The unbiased
163 reference is taken from the AMIP dataset.
164 The land use is prescribed for each year using the Land Use Harmonization 2 (LUHv2) (Hurtt et al., 2020) dataset from the
165 Coupled Model Intercomparison Project 6 (CMIP6); we used the historical and SSP5-8.5 scenarios for 1950-2014 and 2015-
166 2100, respectively. Changes in land use include changes in cropland area (see Figs. S1 and S2 in the Supplementary Material).
167 Each year of irrigated area per grid cell is also prescribed with LUHv2, using the same setup (historical scenario (1950–2014)
168 and the SSP5-8.5 scenario (2015–2100)).
169 The average spatial distribution of irrigated fractions for the 2050—2100 period (see Figure 1-a) includes the current hot spots
170 (India, China, Southeast Asia, and the USA) in addition to new hot spots in Africa (Southeast Africa) and South America (Rio
171 de la Plata area). Changes in the irrigated fraction between the future (2100-2050) and the historical (2000-1950) periods show
172 a strong increase in the irrigated fraction in the new hotspots (Africa and South America) and in northern India and Southeast
173 Asia (see Figure 1-b), but Asia remains the main hotspot of irrigated areas (see Figure 2-a).
174 Note that some areas do not depict major changes or that the irrigated area even decreases (Iraq and some areas in the
175 Mississippi River Basin). Additionally, scenario SSP5-8.5 assumes that the ratio of irrigated area to cropland area increases
176 (see Fig. S2), despite an increase in cropland area, indicating a greater role for irrigation in agriculture and food production.
177 To prescribe the factors of facility of access, we used the Siebert et al. (2010a) map of the fraction of irrigated area equipped
178 with surface water, following Arboleda-Obando et al. (2024a). This map is fixed and representative of conditions around the
179 year 2000. This means that there is no adaptation process related to changes in infrastructure, such as a shift from surface water
180 use to groundwater use.
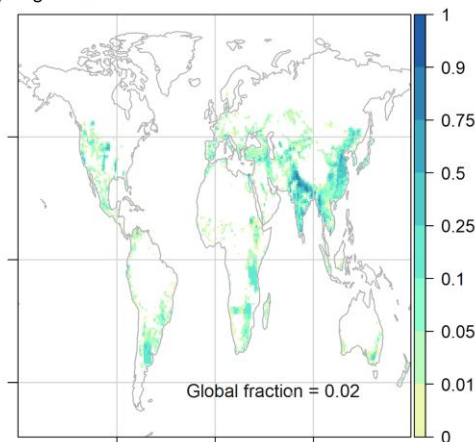
181
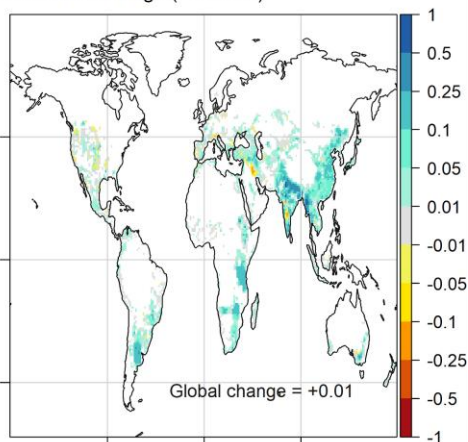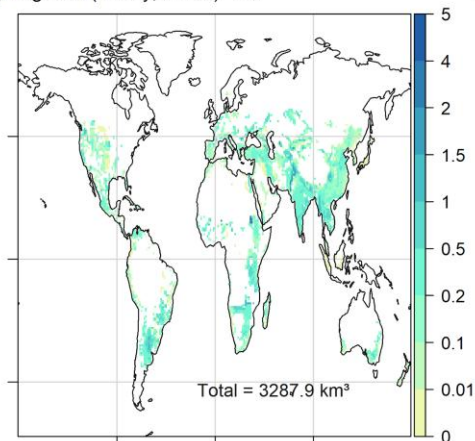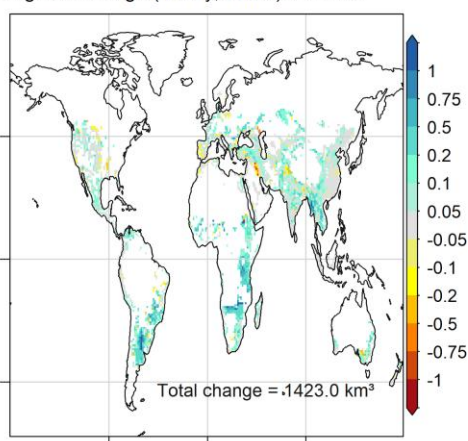
Figure 1: (a) Map of the average irrigated fraction by grid cell for the future period (2050-2100). (b) Map of the change in the average irrigated fraction by grid cell between the future (2050-2100) and historical (1950-2000) periods. The white areas correspond to grid cells with no irrigated fraction. The irrigated fractions are prescribed by the LUHv2 dataset and interpolated to the model resolution. (c) Map of the yearly average irrigation for the future period (2050-2100). (d) Map of the change in the yearly average irrigation amount between the future (2050-2100) and historical (1950-2000) periods. The white areas correspond to grid cells with no irrigation.

188

189
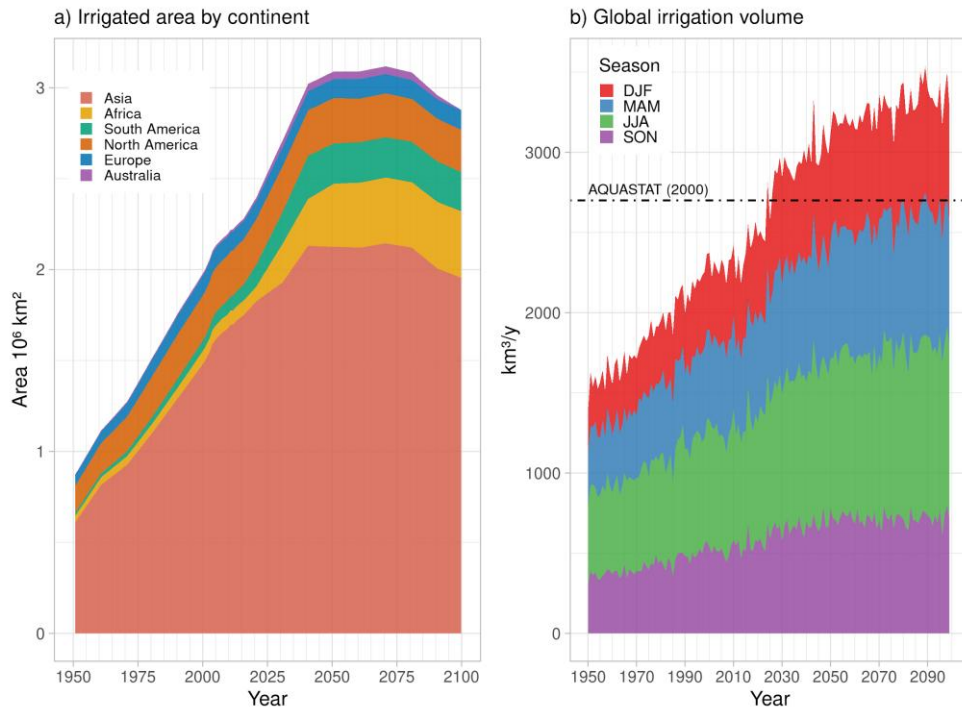
Figure 2: (a) Total irrigated area and by continent prescribed by LUHv2. (b) Total and seasonal irrigation volume at the global scale simulated by IPSL-CM6 in the Irr simulation. The black line represents the value reported by AQUASTAT around the year 2000 (Frenken and Gillet, 2012)**.**

2.4 Analysis tools

We focused on average changes over land, in irrigated areas and in non-irrigated areas, for irrigation as well as important land and atmospheric variables related to the water cycle. Land refers here to all continental areas except Greenland and Antarctica, which are not represented by the ORCHIDEE LSM. We considered that a grid cell belongs to the "irrigated areas" if the average irrigated fraction from 1950-2100 was different from zero (see shaded grid cells in Figure 1a and b) or to the "non-irrigated areas" if the average irrigated fraction was equal to zero for the same period (see white grid cells in Figure 1a and b). We analyze here three main changes on the basis of the differences between the two simulations and between two different periods:

1. The climate change impact is defined by the difference, for a given simulation (Irr or NoIrr), between the future and historical periods (Fut and Hist, set here as 2050-2100 and 1950-2000, respectively). In the following, the impact of climate change is assessed mainly on the basis of the Irr simulation, i.e., Irr(Fut) - Irr(Hist).

2. The influence of irrigation during a given period is identified as the difference between the Irr and NoIrr simulations for a given period. In the following, the influence of irrigation, such as Irr(Fut) - NoIrr(Fut), is assessed in the future period because the influence of irrigation is stronger in the future period (Section 3.2).

3. Since the evolutions of irrigation and climate are coupled in the Irr simulation, we finally introduce a coupling metric, called modulation. This modulation can be described as the effect of irrigation on the alterations produced by climate change, i.e., [Irr(Fut) - Irr(Hist)] - [NoIrr(Fut) - NoIrr(Hist)], but this modulation is equivalent to the effect of climate change on the alterations produced by irrigation, i.e., [Irr(Fut) - NoIrr(Fut)] - [Irr(Hist) - NoIrr(Hist)]. This modulation term is similar to the one introduced in Arboleda Obando et al. (2022) to characterize the coupled changes of climate change and hillslope flow on the basis of trends. While in this study there is no representation of hillslope flows, the concept of modulation is still useful to understand the dynamic interaction between a processus in the continental component of the climate model, and a changing climate.

The statistical significance of the average differences between the two periods (for climate change impacts and modulation) and between the simulations (for irrigation influence) was evaluated with a Student's t test at the 5% significance level.

3 Results

3.1 Evolution of irrigation under a changing climate

In the SSP5-RCP8.5 framework, irrigation continues to increase throughout the simulation period (+76% in the future, for years 2050-2100; compared with the historical period, 1950-2000). At the seasonal scale, global irrigation increases for all four seasons, and the relative weight of each season is not markedly changed throughout the simulation period, although the weight of DJF increases slightly to the expense of MAM; JJA remains the main irrigation season (see around 1000 km³, Figure 2-b). This is consistent with Asia remaining the main irrigation hotspot despite irrigation expansion in Africa and South America (which are located in the southern hemisphere). For the future period, irrigation uses a volume of 3280 km³ (compared with 2700 km³ reported by AQUASTAT around the year 2000), and the most intensively irrigated areas correspond to the Indus and Ganges River Basins, the Nile River Basin, and Southeast Asia River Basins (Mekong, Yellow River, and Yangtze; see Figure 1-c).

The map of the differences between the future and historical irrigation rates (Figure 1-d) reveals a more contrasting distribution. We observe three main classes: first, areas with an increase in irrigation (southern and central Africa, southern South America, Southeast Asia); second, areas with no major change in the irrigation rate (e.g., China, southern India, and central USA); and third, areas with decreasing irrigation (e.g., the Iberian Peninsula, Iraq, and the Mississippi River Basin). The relationship between a decreasing irrigated area and a decreasing irrigation rate is clear in some areas (see the Mississippi River Basin and

233   Iraq); however, other areas are less irrigated despite the expansion of irrigated areas (see areas in the upper Indus river basin,

234   in the lower Ganges river basin and in the Iberian Peninsula). Additionally, an important increase in the irrigated area does not

235   necessarily translate to an important increase in irrigation, as seen in China. This means that climate factors could contribute

236   to explain the evolution of irrigation. But it should be noted that model choices, such as the use of global parameters, a

237   simplified representation of irrigation and the lack of crop phenology, can influence the magnitude or even the sign of water

238   demand and thus the evolution of irrigation.

239

240   **3.2 Average changes and modulation**

241   Table 1 shows the average values from both simulations of 10 key hydroclimate variables, the influence of irrigation and

242   climate change impact on those variables, and the modulation for land, irrigated areas and non-irrigated areas. In section 3.4

243   we assess the spatial distribution of the influence of irrigation for P, ET and water resources. Climate change accelerates the

244   water cycle, warms the air, and increases net radiation. We observe that the influence of irrigation (i.e. the difference between

245   the NoIrr and the Irr simulations) increases the average land values of ET, precipitation (P), runoff (R), and LAI (+4%, +1%,

246   +2% and +3%, respectively), while it depletes water storage in irrigated areas, i.e., groundwater storage (GWS, -7%) and

247   stream storage (Stream S, -8%), but increases water storage in non-irrigated zones (+2% for GWS). The influence of irrigation

248   on total water storage (TWS) on average land values is positive (+0.7%), which is partially due to an increase in soil moisture

249   (SM, +1% over land).

250   In the case of water-related variables and the LAI, the effect is stronger in irrigated areas, but there is a positive effect in non-

251   irrigated areas owing to a positive atmospheric response that increases P by approximately 1% under historical and future

252   climates. On the other hand, the influence of irrigation is positive for net radiation and negative for air temperature at 2 m (Tas)

253   and is confined to irrigated areas. Changes in radiation variables are explained by evaporative cooling and a decrease in

254   longwave radiation emission, which increases the net radiation.

255   Modulation is important in irrigated areas for the ET, R, and water storage variables but rather weak in non-irrigated areas.

256   For example, irrigation increases ET by 8% under historical conditions and by 12% under future climate conditions in irrigated

257   areas, which means that irrigation accelerates the increase in ET induced by climate change in the Irr simulation. Net radiation

258   and air temperature evolution are also affected by irrigation in irrigated areas, but there is no major change in the evolution in

259   non-irrigated zones when comparing Irr and NoIrr. On the other hand, the influence of irrigation on the precipitation evolution

260   is negligible in both irrigated and non-irrigated areas.

261   **3.3 Climate change impacts**

262   The spatial distributions of the impacts of climate change on precipitation and air temperature are shown in Figure 3-a and b

263   (see Fig. S3 for the spatial distributions, including those of the oceans). In irrigated areas, precipitation may either increase

264   due to climate change (e.g., China and southern India, with local extremes of more than +1 mm/day) or decrease

265 (Mediterranean area, with local extremes in the Iberian Peninsula below -1 mm/day), whereas warming occurs in all areas.

266 These changes in climate can contribute to changes in irrigation: positive changes in precipitation can increase available water

267 and water resources while decreasing the soil moisture deficit and water demand. Negative changes in precipitation increase

268 water demand, which could increase irrigation if water resources are available. Warming tends to increase water demand, but

269 it should be noted that warming tends to be greater in northern latitudes (warming above 7 °C) than in tropical and southern

270 areas (warming above 3 °C) as a result of the land warming pattern, visible in non-irrigated areas (see Figure 3-b).

271 The impacts of climate change present similar spatial distributions to those of other hydrologic variables, with some differences

272 (see Figure 4). ET increases in the future compared with the historical period in the Irr simulation (Figure 4-a), with major

273 exceptions in a few tropical regions (central Africa and parts of the Amazon River basin) and at higher latitudes (the Iberian

274 Peninsula and southern Australia) owing to changes in net radiation and precipitation, respectively. The impact of climate

275 change on runoff (R, Figure 4-b) follows a spatial pattern similar to that of P changes, with some exceptions in North America.

276 Finally, climate change impacts on water storage, i.e., GWS and Stream S (Figure 4-c and d), follow the spatial patterns of P.

277 Note that there are exceptions for GWS in irrigated areas such as the central U.S. and South Asia, which depict negative

278 changes even if precipitation increases. Additionally, the strongest changes in stream reservoirs are found in grid cells

279 containing the largest rivers, since changes in the stream water budget of any grid cell propagates along the river network, and

280 accumulate in the grid cells with large upstream areas (e.g. Amazon river, Nile river, Congo river and Indus river). The next

281 step is to assess in more detail the influence of irrigation on key hydroclimate variables.

282

283

Table 1: Yearly average values over land, irrigated areas and non-irrigated areas for 10 variables related to hydroclimate surface conditions. The considered values by variable are the average in the irr simulation for a chosen period (Hist, 1950-2000 and Fut, 2050-2100), the influence of irrigation by period, the effect of climate change in the Irr simulation, and the modulation. The values in bold marked with an * correspond to a p value under 0.05 according to Student's t test.

Variable (yearly)	Simulation	All land			Irrigated regions			Non-irrigated regions		
		1950-2000	2050-2100	Fut-Hist	1950-2000	2050-2100	Fut-Hist	1950-2000	2050-2100	Fut-Hist
ET, mm/d	Irr	1.66	1.72	**0.06 (3%)***	1.9	2.1	**0.2 (7.9%)***	1.57	1.6	**0.03 (2%)***
	NoIrr	1.62	1.66	**0.04 (2%)***	1.75	1.85	**0.1 (3.1%)***	1.56	1.59	**0.03(2%)***
	Irr-NoIrr	**0.04 (2%)***	**0.06 (4%)***	**0.02 (57%)***	**0.15 (8%)***	**0.25 (12%)***	**0.1 (65%)***	**0.008 (0.5%)***	**0.009 (0.6%)***	0.001 (12.4%)
P, mm/d	Irr	3.04	3.29	**0.25 (8%)***	3.16	3.43	**0.27 (9%)***	3	3.25	**0.25 (8%)***
	NoIrr	3.04	3.29	**0.25 (8%)***	3.16	3.43	**0.27 (9%)***	3	3.25	**0.25 (8%)***
	Irr-NoIrr	**0.03 (0.9%)***	**0.04 (1%)***	0.01 (30%)	**0.04 (1%)***	**0.05 (1.4%)***	0.01 (38%)	**0.03 (0.9%)***	**0.04 (1%)***	0.01 (26%)
GWS, mm	Irr	34.7	41.5	**6.8 (20%)***	35	37	**2 (6%)***	34.5	42.8	**8.3 (24%)***
	NoIrr	35	42	**7.0 (20%)***	37.5	42.5	**5 (12%)***	34.1	41.9	**7.8 (23%)***
	Irr-NoIrr	-0.3 (-0.7%)	**-0.5 (-1%)***	-0.2 (85%)	**-2.5 (-7%)***	**-5.5 (-14%)***	**-3 (102%)***	**0.4 (1%)***	**0.9 (2%)***	0.5 (115%)
Stream S, mm	Irr	7	8.7	**1.7 (24%)***	6.8	8.3	**1.5 (22%)***	7.14	8.88	**1.74 (24%)***
	NoIrr	7.1	8.9	**1.8 (26%)***	7.4	9.3	**1.9 (26%)***	7.07	8.88	**1.8 (25%)***

	Irr-NoIrr	-0.08 (-1%)*	-0.2 (-3%)*	-0.12 (186%)*	-0.6 (-8%)*	-1 (-12%)*	-0.4 (81%)*	0.062 (0.9%)	0.002 (0.02%)	-0.06 (-97%)
R, mm/d	Irr	1.42	1.64	**0.22 (16%)***	1.37	1.6	**0.23 (17%)***	1.43	1.65	**0.22 (16%)***
	NoIrr	1.4	1.61	**0.21 (15%)***	1.33	1.53	**0.2 (15%)***	1.41	1.63	**0.22 (15%)***
	Irr-NoIrr	**0.02 (2%)***	**0.03 (2%)***	**0.01 (54%)***	**0.04 (3%)***	**0.07 (4%)***	**0.03 (87%)***	**0.02 (1%)***	**0.03 (2%)***	0.01 (35%)
LAI, m²/m²	Irr	1.47	1.9	**0.43 (29%)***	1.5	2	**0.5 (34%)***	1.45	1.85	**0.4 (27%)***
	NoIrr	1.44	1.85	**0.41 (28%)***	1.4	1.8	**0.4 (31%)***	1.45	1.84	**0.39 (27%)***
	Irr-NoIrr	**0.03 (2%)***	**0.05 (3%)***	**0.02 (94%)***	**0.1 (6%)***	**0.2 (9%)***	**0.1 (82%)***	**0.004 (0.3%)***	**0.012 (0.7%)***	**0.008 (169%)***
SM, mm	Irr	493.5	498.5	**5 (1%)***	498	505	**7 (1%)***	492	496	**4 (0.8%)***
	NoIrr	490	493	**3 (0.7%)***	490	490	0.01 (0.003%)	489.9	494	**4.1 (0.9%)***
	Irr-NoIrr	**3.5 (0.8%)***	**5.5 (1%)***	**2 (40%)***	**8 (1.7%)***	**15 (3%)***	**7 (85%)***	**2.1 (0.5%)***	**2 (0.5%)***	**-0.1 (-6%)***
TWS, mm	Irr	690	706	**16 (2%)***	692	713	**21 (3.0%)***	689	704	**15 (2%)***
	NoIrr	686	701	**15 (2%)***	685	703	**18 (2.7%)***	686.2	700.8	**14.6 (2.1%)***
	Irr-NoIrr	**4 (0.6%)***	**5 (0.7%)***	1 (22.6%)	**7 (1%)***	**10 (1%)***	**3 (34%)***	**2.8 (0.4%)***	**3.2 (0.5%)***	0.4 (14%)
Net rad., W/m²	Irr	90	95	**5 (5%)***	100	105	**5 (5%)***	86.9	91.8	**4.9 (6%)***

	NoIrr	89.6	94.4	**4.8 (5%)***	98.4	102.6	**4.2 (4%)***	86.8	91.8	**4.9 (6%)***
	Irr-NoIrr	**0.4 (0.5%)***	**0.6 (0.6%)***	**0.2 (38%)***	**1.6 (2%)***	**2.4 (2%)***	**0.8 (54%)***	0.08 (0.09%)	0.04 (0.04%)	-0.04 (-49%)
	Irr	13.5	19.1	**5.6 ***	16.5	21.5	**5 ***	12.5	18.3	**5.8 ***
Tas, ℃	NoIrr	13.5	19.2	**5.7 ***	16.7	21.9	**5.2 ***	12.5	18.4	**5.9 ***
	Irr-NoIrr	**-0.09 ***	**-0.14 ***	-0.05 (57%)	**-0.2 ***	**-0.4 ***	**-0.2 (66%)***	-0.05	**-0.07 ***	-0.02 (44%)

288

289
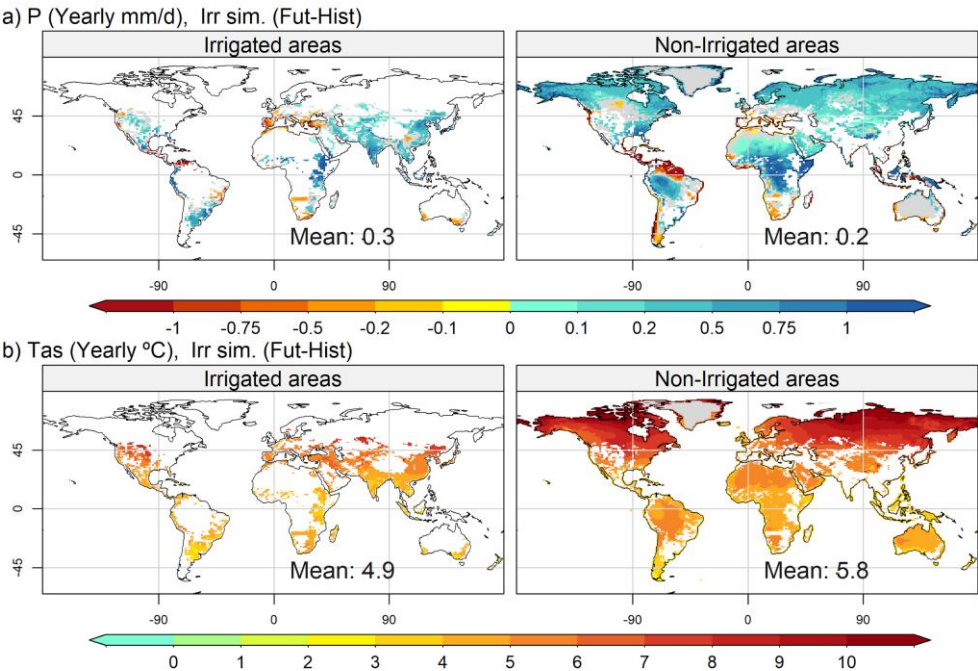
290 **Figure 3: Map of the spatial distribution of yearly changes between future and historical periods for irrigated areas (left column)**
291 **and non-irrigated areas (right column), for precipitation (a) and air temperature at 2 meters (b). The areas in gray correspond to a**
292 **p value less than 0.05 according to Student's t test.**

293

294
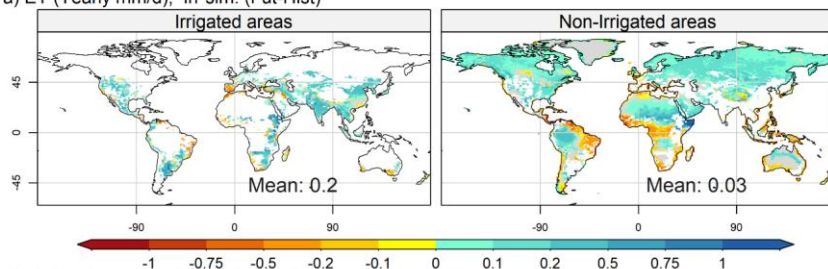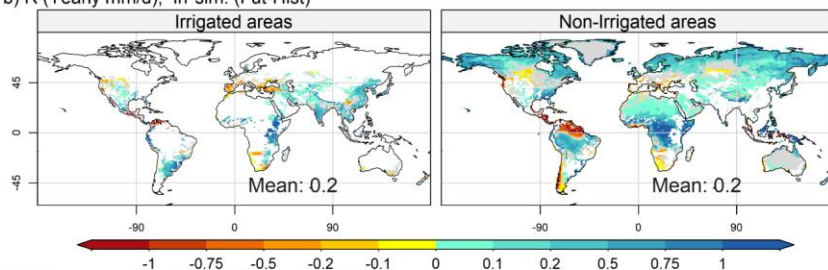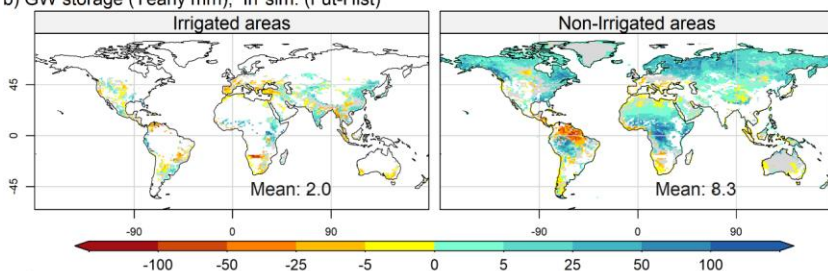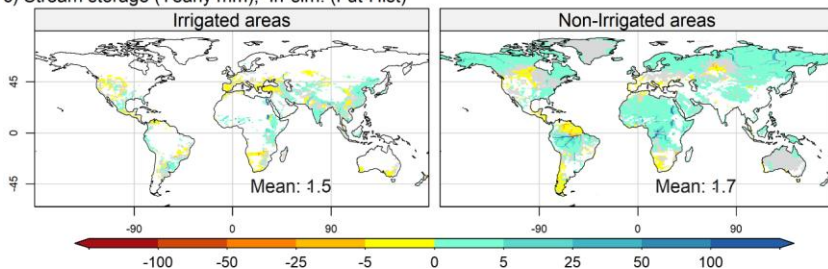
Figure 4: Map of the spatial distribution of yearly changes between future and historical periods for irrigated areas (left column) and non-irrigated areas (right column), for evapotranspiration (a) total runoff (b), groundwater reservoirs (c) and stream reservoirs (d). The areas in gray correspond to a p value under 0.05 according to a Student's t-test.

3.4 Irrigation influence

The evolution of the ET and P yearly average rates over land, for irrigated areas and non-irrigated areas, as defined in section 2.4, is shown in Figure 5. For ET, the NoIrr simulation shows a decreasing trend in irrigated areas (from 1.81 mm/d during 1950-1975, to 1.79 mm/d during 1975-2000) during the 1950-2025 period that is not present in the Irr simulation (see Figure 5a, second row). Additionally, the changes in ET observed over land (see Figure 5a, first row) are driven by changes in irrigated areas (+0.15 mm/d in historical, +0.25 mm/d in future), as the ET values in non-irrigated areas are similar for both simulations (see Figure 5a, third row). Finally, we observe that the increase in ET in irrigated areas after 2025 is faster in the Irr simulation than in the NoIrr simulation, even though irrigation expansion stops by 2040 (Figure 2-a). In the case of P, irrigation activities increase the yearly average values over land around 0.04 mm/d (Figure 5b, first row) and in irrigated areas (Figure 5b, second row), but there is no major influence on the evolution over time (both NoIrr and Irr simulations show a similar positive trend over the period). This means that the positive trend in precipitation over land (Figure 5b, first row) is driven by other forcings, i.e., climate change and land use and land cover change.

Figure 6 shows the spatial distribution of the influence of irrigation (Irr-NoIrr) in the future for ET and P. In the future period, irrigation always increases ET in irrigated areas (with local extremes in the Indus river basin above +1 mm/d), and in many non-irrigated areas nearby (Figure 6-a, especially in central Asia and the African Sahelian band, with values below +0.1 mm/d). We also note non-irrigated areas where ET decreases in the future in the Irr simulation (Russian tundra, some areas in central Africa), involving negative feedback loops between P and ET changes via net short-wave radiation (not shown): in these areas, P increases, either statistically significantly or not, which increases cloudiness and reduces downwelling short-wave radiation, thus reducing ET, as already described in central Africa by Wang et al. (2018); in Northern Russia, the P increase can also lead to increased snowfall and surface albedo, reducing available energy for ET.

Like for ET, irrigation mostly increases P, over both irrigated and non-irrigated areas, but on smaller surfaces (Figure 6-b, with values below +0.5 mm/d; the same figure including the oceans is shown in Fig. S3). The joint increase of ET and P in non-irrigated areas around irrigated areas reveals a remote impact of irrigation linked to atmospheric transport of moisture from irrigated to surrounding areas, which supports higher P and therefore higher ET in non-irrigated areas, such as the Sahelian band and Central Asia. Changes in P farther away from irrigated areas are rare and may result from various atmospheric processes in a generally more humid atmosphere.

The modulation is mostly positive for ET in irrigated zones (indicating that the influence of irrigation on ET is more important in the future; see Fig. S4-a) and is similar to the evolution observed for LAI (see Fig. S5 and S6). For P, the modulation is weak (see Fig. S4-b for P). The influence of irrigation on other variables is consistent with these changes (see Fig. S5 and S6 for R; Fig. S7 and S8 for TWS and SM; Fig. S9 and S10 for net radiation and Tas).
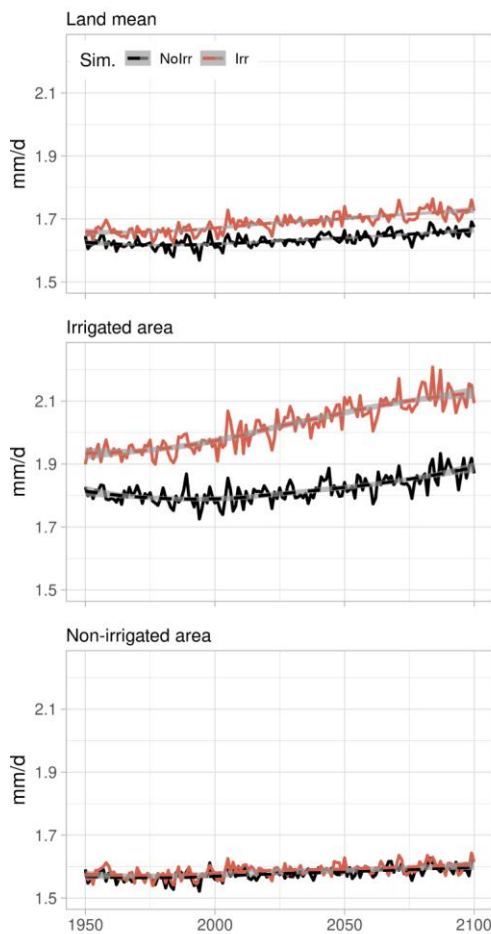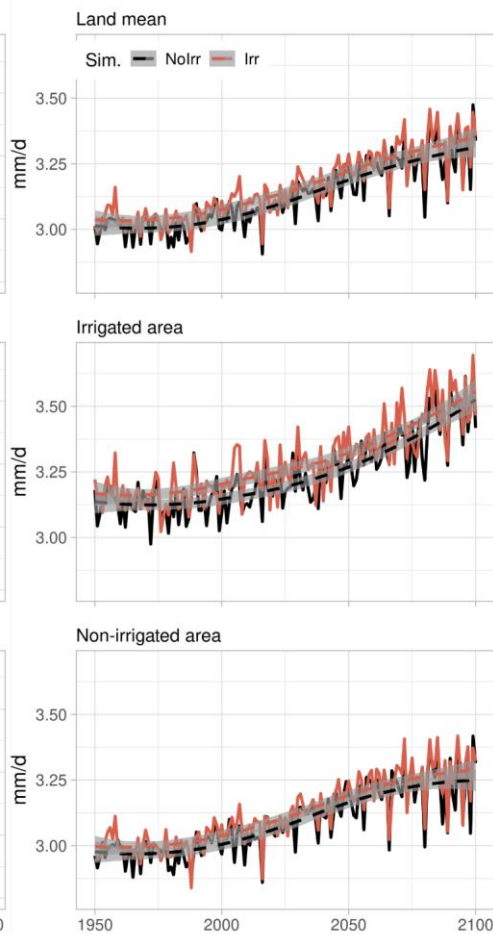
Figure 5: Time series of yearly evapotranspiration (a, left column) and precipitation (b, right column). The first row corresponds to averages over land, the second row corresponds to averages over irrigated areas, and the third row corresponds to averages in non-irrigated areas. The dashed lines correspond to a fitted polynomial curve via local fitting.

a) Irr-NoIrr, ET (Yearly mm/d): Fut

b) Irr-NoIrr, P (Yearly mm/d): Fut

336
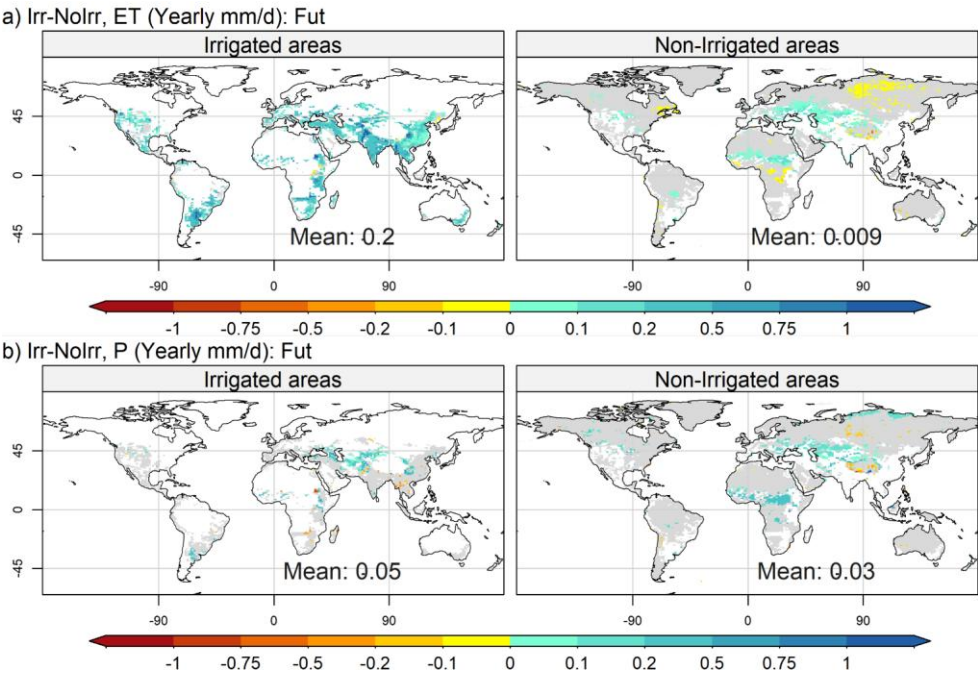
337 **Figure 6: Map of the spatial distribution of yearly changes between the Irr and NoIrr simulations under future climate conditions**
338 **for irrigated areas (left column) and non-irrigated areas (right column), for evapotranspiration (a) and precipitation (b). The areas**
339 **in gray correspond to a p value less than 0.05 according to Student's t test.**

340

341 Time series of water storage in groundwater (which represents shallow aquifers, see Figure 7a) and stream (which represents

342 large rivers, see Figure 7b) reservoirs show important differences between NoIrr and Irr simulations. These differences are

343 explained by complex interactions between irrigation activities, climate conditions, and water resources (see differences over

344 land, Figure 7 first row; irrigated areas, Figure 7 second row; and non-irrigated areas, third row) that we pass to show. The

345 impact of climate change induces a positive trend in water storage (Figure 7-a and b, first row), whereas irrigation decreases

346 the average GWS and Stream S in irrigated areas in around -14 and and -12% in the future, respectively (Figure 7-a and b,

347 second row) and slightly increases the GWS and Stream S in non-irrigated areas in around +2 and +0.02% in the future,

348 respectively (Figure 7-a and b, third row). The negative effects in irrigated areas are explained by direct water use to sustain

349 irrigation activities, whereas the increase in water resources in non-irrigated areas in the Irr simulation is explained by the fact

350 that irrigation increases precipitation remotely, in particular around irrigated zones (Figure 6b, right panel). The modulation is

351 also negative in irrigated areas (i.e., water resource exploitation increases) but weak in non-irrigated areas. Note that the effect
352 of irrigation on water storage reservoirs seems to counteract the increase induced by climate change in irrigated areas before
353 2040, and after 2040 the increase of water storage (groundwater and stream reservoirs) is slower in the Irr simulation than in
354 the NoIrr simulation.
355 Figure 8 depicts the spatial distribution of the influence of irrigation in the future for GWS and Stream S. The effects are
356 mostly negative for both variables in irrigated areas, but in the case of Stream S, depletion is more important in the grid cells
357 containing large rivers (with local extreme values under -50 mm in the Indus and Rio de la Plata rivers) because the influence
358 of irrigation propagates through the river system. Additionally, the modulation is mostly negative for both reservoirs (with
359 some local exceptions in the GW reservoir), indicating that the water use intensity increases during the simulated period (see
360 Fig. S4-c and d).
361
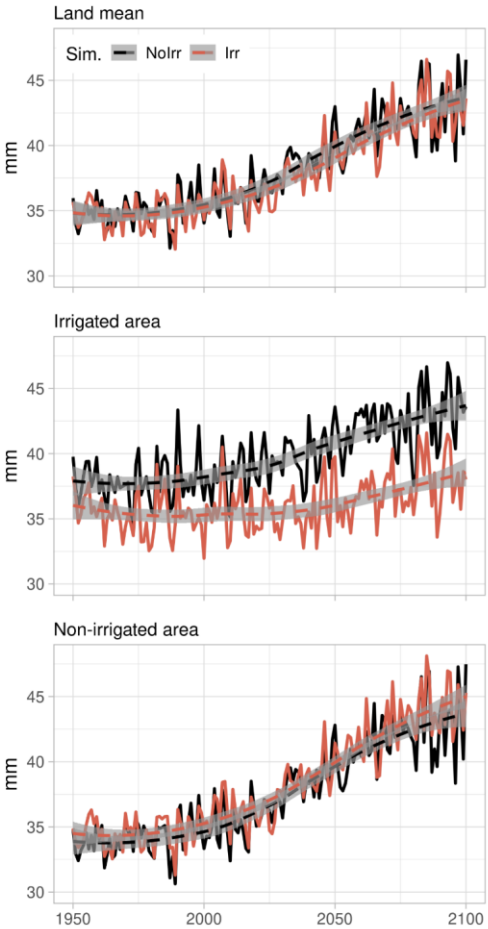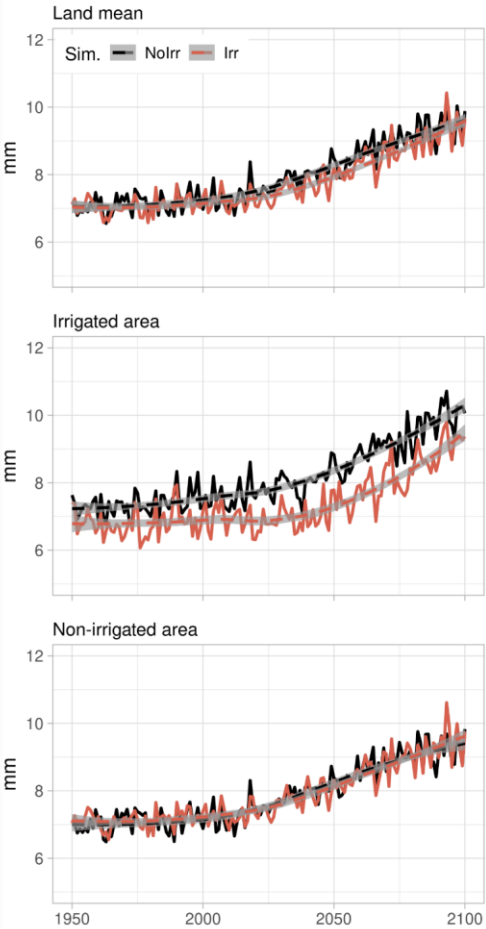
Figure 7: Time series of yearly groundwater storage (a, left column) and stream storage (b, right column). The first row corresponds to the average on land, the second row corresponds to the average in irrigated areas, and the third row corresponds to the average in non-irrigated areas. The dashed lines correspond to a fitted polynomial curve via local fitting.

a) Irr-NoIrr, GW storage (Yearly mm): Fut

b) Irr-NoIrr, Stream storage (Yearly mm): Fut
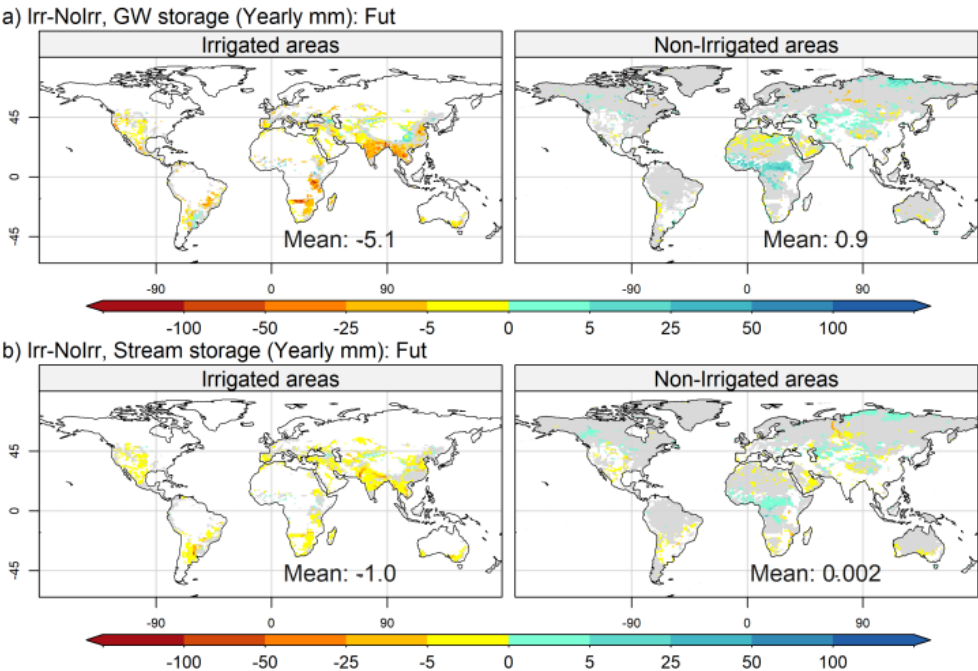
Figure 8: Idem as in Figure 6 for groundwater storage (a) and stream storage (b). The areas in gray correspond to a p value less than 0.05 according to Student's t test.

3.5 Joint effects of irrigation and climate change on river discharge

River discharge integrates all changes linked to climate change and irrigation at the basin scale. We decide to analyze the effects on yearly average values in the 50 largest river basins (~~see~~ Table S1), and we present monthly average discharge values of seven river basins that summarize the results obtained (~~see~~ Figure 9). We classify changes in river discharge into three classes, based on three variables: the average irrigated fraction during a period (historical or future), the effect of climate change on discharge, and the irrigation influence on discharge.

The first class corresponds to large river basins with heavy irrigation activities, i.e. with an average irrigated fraction higher than 1% during the historical or future period (illustrated by the Nile, Rio Grande, Indus and Ganges; ~~see~~ Figure 9-a, b, c, and d). In these river basins, irrigation activities decrease discharge values throughout the year (decrease in the future due to irrigation ranges between -4 up to -51% of discharge) under both historical and future climate conditions, with no major changes in seasonality (except in Rio Grande). The impact of climate change increases the discharge values in the future, and

380 the decrease of discharge by irrigation is greater in the future than in the historical period, because the irrigated fraction
381 increases, boosting the demand, and the increased water supply by river discharge allows irrigation withdrawals to follow the
382 demand.
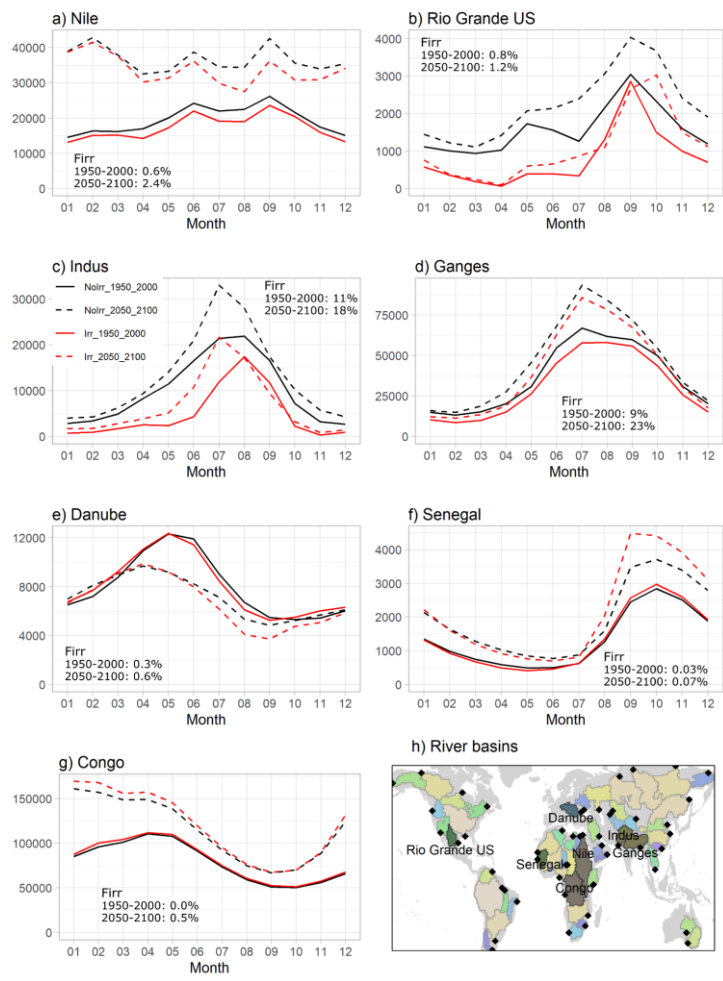
383

Figure 9: Monthly multiyear values of discharge (m³/s) at the basin outlet in the chosen river basins (a-g) and the 50 river basins considered in the analysis (h), with highlights of the rivers presented in a-g.

The second class is illustrated by the Danube River basin (Figure 9-e, as well as the Dnepr and Nelson river basins, ~~see~~ Table S1), and corresponds to river basins with modest irrigation activities (i.e. average irrigated fraction lower than 1% during the historical or future period) and a decrease of river discharge with climate change (decrease due to climate change range from -1 up to -15% of discharge). Under the historical climate (solid lines) conditions, river discharge from the Irr simulation increases during the winter months compared with that from the NoIrr simulation (owing to a positive P change in the area), but discharge values from the Irr simulation are lower than those from the NoIrr simulation during the summer (when water resources are used to sustain irrigation activities). Under the future climate, the positive difference during the winter is weaker, whereas the negative difference during the summer is greater (due to the regional decrease in P and increase in ET due to climate change and the increase in effective irrigation).

The third class also corresponds to river basins with modest irrigation activities (irrigated fraction lower than 1%) in both periods, but a slightly positive influence of irrigation on discharge (increase in the future ranges between +3 to +12%). This class is illustrated by two African river basins: the Congo and Senegal river basins (~~see~~ Figure 9-f and g). Both basins show slightly higher discharge values for the Irr simulation than for the NoIrr simulation under the historical climate, and this positive difference is greater under the future climate scenario. The positive influence of irrigation under the historical climate is explained by the P increase in non-irrigated areas of both river basins in the Irr simulation. On the other hand, the greater influence of irrigation under the future climate than under the historical climate can be explained by the negative impact of climate change on ET in the area (~~see~~ Figure 4) and the positive modulation of P in some areas of the Sahelian band (indicating more P in the Irr simulation in the future; ~~see~~ Figure S4). Notably, positive modulation occurs during the wet season in both cases, and in the case of the Congo River basin, the modest irrigation expansion (the irrigated area increases from 0 to 0.5%) does not decrease discharge in the future, despite an increase in irrigation (~~see~~ Figure 1-d).

3.6 Hydroclimate limits to irrigation growth

We showed that irrigation has an important influence on the evolution of the water cycle and water resources in irrigated areas. This influence is modulated by the expansion of irrigated areas and can enhance the effects of climate change or reduce them, depending on local conditions. However, we have not yet analyzed whether climate change impacts can explain changes in irrigation, which could in turn modulate the influence of irrigation on the water cycle and water resources. To analyze this type of interaction, we show a map of classes according to the joint changes in precipitation and irrigation in Figure 10-a and according to the joint changes in irrigation and GWS in Figure 10-b. We also show boxplots of average changes by class for key hydroclimate variables in Figure 11.

We can observe that the areas where precipitation decreases correspond to roughly one-fifth of the total irrigated areas (red and orange classes in Figure 10-a). In the orange zones, irrigation increases in response to a larger irrigated fraction, drier soil, and higher net radiation (which increases the water demand, ~~see~~ Figure 11), increasing irrigation as a trade-off between less

417 available water and more water demand. In the red zones, due to the shortage of water supply, irrigation cannot increase even
418 if the irrigated surface increases in many zones (approximately half of the grid cells; see Figure 11), the soil is drier, and the
419 net radiation increases.
420 The difference in available water for irrigation explains the significant decrease in GWS in the orange zones due to the
421 combined effect of less P and greater water withdrawal, whereas in the red areas, the decrease in GWS is close to zero, as it is
422 not possible to further increase water withdrawal, which is near the maximum under the historical climate. The effects of
423 changes in irrigation also explain the differences in ET changes and LAI changes between the red and orange classes.
424 Additionally, the decrease in the irrigated fraction, which might decrease the irrigation demand and effective irrigation, plays
425 a minor role in the case of the red class.
426 Areas with increased precipitation account for four-fifths of the total irrigated area (green and blue classes in Figure 10-a). In
427 the green areas, effective irrigation decreases, in part because the irrigated fraction decreases in many areas (slightly less than
428 half of the grids, see Figure 11; this class includes Iraq and the Mississippi River Basin where Firr decreases, see Figure 10-b)
429 but also because the climate change increase in soil moisture and net radiation is less important than in the blue class (for
430 example, in some areas of China).
431 In the blue areas, irrigation increases (e.g., in China and India), partly because the irrigated fraction increases and because the
432 increase in net radiation is more important (which increases water demand) despite the increase in soil moisture (which
433 decreases water demand). These differences in SM and net radiation partly explain the differences in the changes in ET and
434 LAI, which increase more in the areas classified as blue than in those classified as green. In addition, the areas classified as
435 green could present a potential for the expansion of irrigated systems (if there is available space for agriculture) or even for
436 the use of rainfed systems if the future local climate allows it. But such policy decisions often depend on other socio-economic
437 factors beyond environmental conditions (Mehta et al., 2024; Petit et al., 2017; Siebert et al., 2015).
438 With respect to the relationship with water resources, the blue and green areas generally show an increase in GWS, indicating
439 an increase in water resources (see Figure 11). However, in at least a quarter of the areas classified as blue, GWS decreases
440 and irrigation increases despite the increase in P (i.e., some grid cells are classified as blue in Figure 10-a but as orange in
441 Figure 10-b). This indicates that increased irrigation leads to a depletion of water resources, even under a wetter climate. In
442 total, areas where changes in climate or irrigation intensity lead to water resources depletion (classes red and orange in Figure
443 10-b) constitute one third of the total irrigated area and include the intensively irrigated areas of northern India and Southeast
444 Asia. A direct consequence is that areas classified as orange in Figure 10-b (less water storage while irrigation increases) may
445 face more tension over water use because of overexploitation of water resources (in those areas where P increases) or due to
446 the trade-off between less rainfall and more water demand, while red areas in Figure 10-b may face a decline of irrigation
447 activities due to the shortages of water supply.

a) Joint changes of P and Irr

P-_Irr-   P-_Irr+   P+_Irr-   P+_Irr+
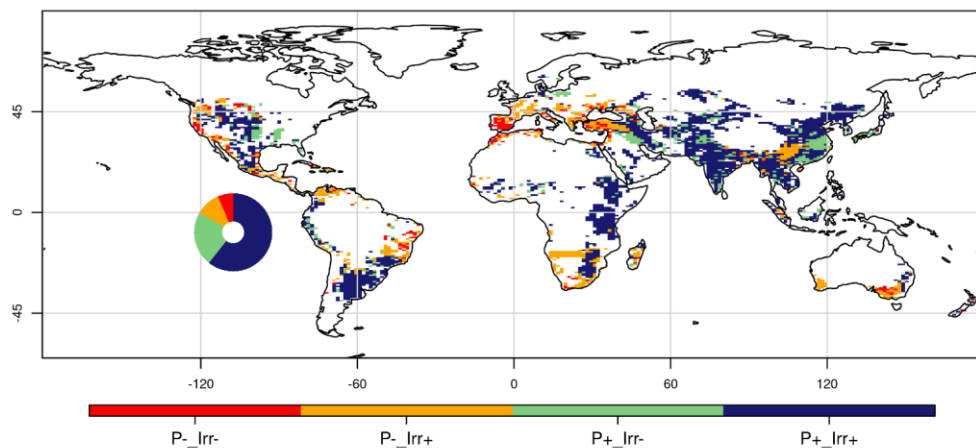
b) Joint changes of Irr and GWS

Irr-_GWS-   Irr+_GWS-   Irr-_GWS+   Irr+_GWS+
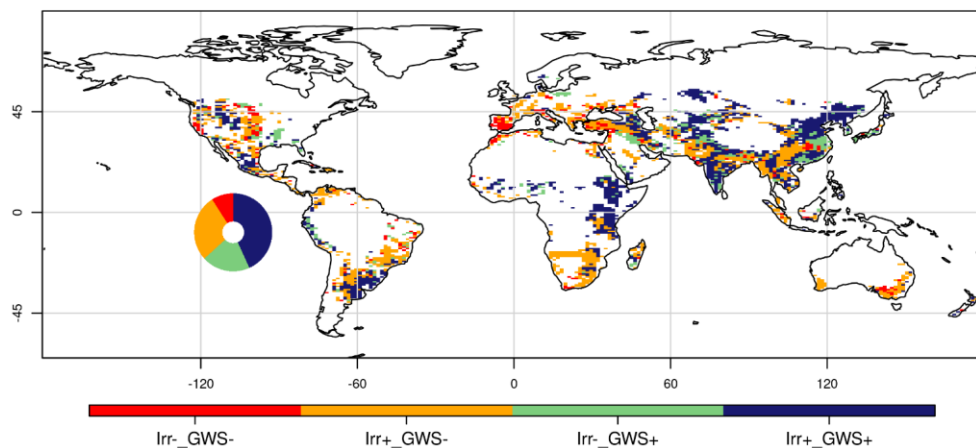
Figure 10: Joint changes between the future (Fut, 2050-2100) and historical (Hist, 1950-2000) periods for precipitation (P) and irrigation (Irr) in irrigated areas (a) and for groundwater reservoirs (GWS) and irrigation (Irr) in irrigated areas (b). The symbols + and - indicate positive and negative changes, respectively. The insets indicate the fraction of irrigated area by class.

452
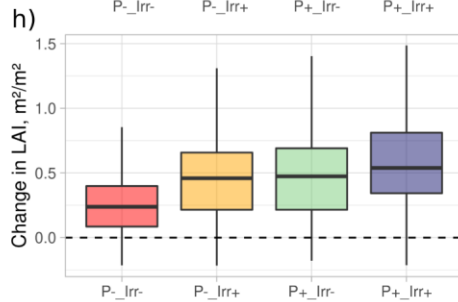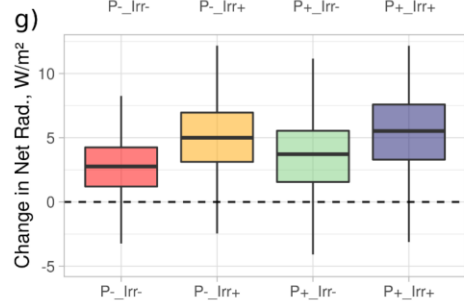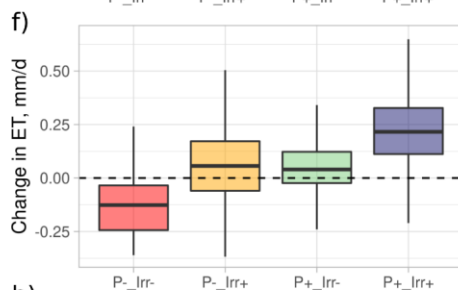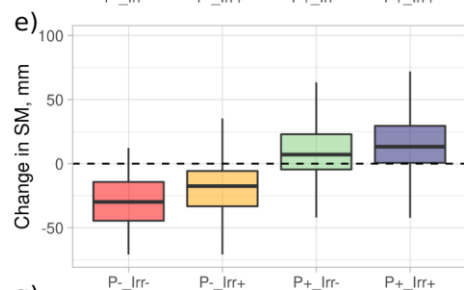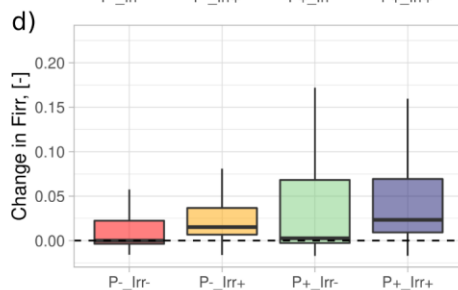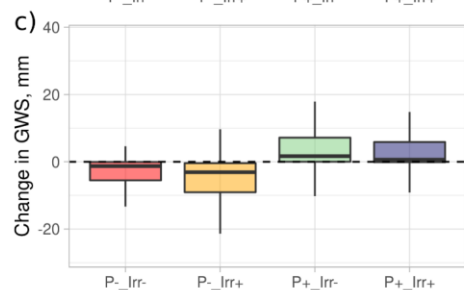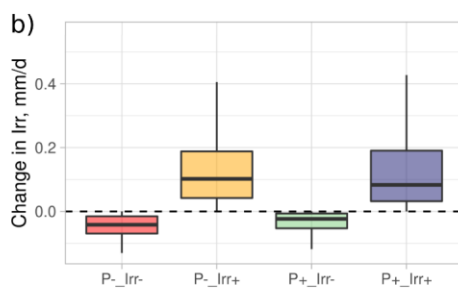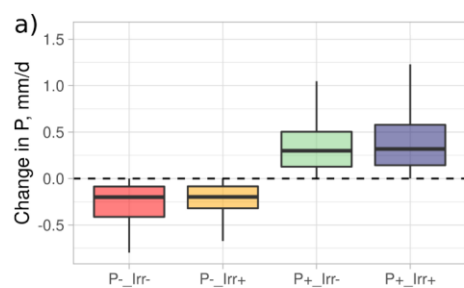
Figure 11: Boxplots of average climate change impacts as simulated in the Irr simulation, in irrigated grid cells classified according to Figure 11-a (joint change in P and Irr), for precipitation (a), irrigation (b), GWS (c), irrigated fraction (d), SM (e), ET (f), net radiation (g), and LAI (h).

4 Discussion

First of all, it is important to recall that our results are framed by several important uncertainties related to our modeling framework:

1. The use of SSP5-8.5 as a single radiative forcing scenario induces a strong warming and significant changes in precipitation. This scenario could be seen as the upper boundary of potential climate change impacts, but the magnitude and spatial distribution of these changes are uncertain (AR6, IPCC, 2021). The direct impact of climate change on irrigation could be affected by this uncertainty, especially with regard to changes in precipitation patterns.

2. The ocean component in our simulation is prescribed, while there is evidence that ocean-atmosphere interactions modulates irrigation impacts (Krakauer et al., 2016).

3. Uncertainty due to internal variability, i.e. the natural variations in climate due to interaction of different components of the Earth System, is not considered, since we use a single simulation instead of an initial-condition ensemble (Schwarzwald and Lenssen, 2022).

4. Some specific processes report uncertainty as well, for instance the response of convective storms to warming (Lepore et al., 2021), the magnitude of some energy balance components, especially latent heat flux (Wild, 2020), or the representation of local breeze circulation at the subgrid scale (Lunel et al., 2024).

5. The evolution of SM-atmosphere coupling in climate projections is uncertain (Qiao et al., 2023; Zhou et al., 2021), especially in regions identified as transition zones with strong land-atmosphere coupling (Koster et al., 2006; Seneviratne et al., 2013) but this uncertainty is not considered since no multi-model ensemble is used.

6. The misrepresentation of subgrid variability in the land surface-atmosphere coupling (de Vrese et al., 2016b), specifically on the energy budget computed by IPSL-CM6, could have an impact on irrigation demand, on atmospheric feedbacks and on irrigation efficiency (de Vrese and Hagemann, 2018).

These uncertainties quantitatively influence the entire simulated water cycle, so that our results are model-specific and must be confirmed using other land-atmosphere models and available observations.

Our results are also strongly dependent on the shortcomings of ORCHIDEE's representation of crop irrigation and its water sources, some of these shortcomings shared with other LSMs (McDermid et al., 2023):

1. The ORCHIDEE LSM lacks a parameterization of deep, non-renewable GW, and the map of water access infrastructure is fixed to year 2000-conditions (Arboleda-Obando et al., 2024). Also, river water adduction is deactivated in the Irr simulations due to the coarse resolution These three shortcomings may reduce the water

485   supply for irrigation, thus limiting the simulated irrigation withdrawal. They call for a massive effort to better
486   account for human water management.

487   2.   Our irrigation parameterization uses flood irrigation as the only irrigation technique worldwide and overlooks local
488   irrigation practices (Arboleda-Obando et al., 2024). Model choices (such as the use of global parameters, simplified
489   irrigation rules, and lack of specific crop phenology) necessarily impact the regional magnitude of water demand
490   and thus the evolution of irrigation. Here again, these shortcomings highlight the need for more complex human
491   water use modules in LSMs (Taranu et al., 2024; Yao et al., 2022).

492   3.   The irrigated crops are also very simplified in our model: our single C3 and C4 crop types follow a natural
493   phenology, without harvest, which probably leads to overestimate the simulated irrigation at the end of the growing
494   season; in contrast, multiple cropping and paddy fields are overlooked, leading to underestimate the simulated
495   irrigation (Arboleda-Obando et al., 2024). The overall effect of these shortcomings are difficult to assess
496   quantitatively, and they are not exhaustive.

497   With these limitations in mind, we analyze how our findings usefully complement those of four important articles on irrigation
498   related trends. Firstly, our conclusions regarding the influence of irrigation on ET and P match those of Cook et al. (2020), but
499   with a more solid framework in our case. The simulations of Cook et al. (2020) benefit from an ensemble of multiple
500   simulations thus better assessing internal variability, but all the simulations include irrigation, so the influence of irrigation is
501   approximated from the comparison of irrigated and nearby non-irrigated areas, where the effect of irrigation on ET and P is
502   assumed to be zero. Our results, albeit based on one member only, show that irrigation significantly increases P and ET in
503   many areas surrounding irrigated regions, so the influence of irrigation estimated by Cook et al. (2020) on these two variables
504   were likely underestimated.

505   Analyzing the atmospheric impact of irrigation in more remote regions is challenging and was not comprehensively addressed
506   in this study. De Vrese et al. (2016a) tackled this issue by carefully studying how wind patterns are modified by irrigation in
507   coupled simulations of historical climate, and showed that irrigation in India leads to increase P in East Africa and Central
508   Asia, owing to water vapor advection and disturbances in the Asian Monsoon. Our results focused on the effects of irrigation
509   on water resources, and therefore the effects on atmospheric circulation were not analyzed in detail, although similar processes
510   may exist in our simulations. A better understanding of the effects of irrigation on precipitation in remote areas must define
511   what a "remote area" means, then analyze the relationship between irrigation (taking into account the intensity and spatial
512   distribution of irrigation), and changes in atmospheric circulation and moisture transport in a given climate (either historical
513   or future). This analysis can be more robustly complemented by the use of inverse trajectory methods (Wei et al., 2013), to
514   estimate the contribution of irrigation to total precipitation, and by the use of water tagging, to track the origin of water vapor
515   and continental recycling (Risi et al., 2013) and study the changes induced by irrigation.

516   Our conclusions regarding irrigation growth at global scale for the period 1950-2100 are in line with irrigation projections
517   based on agronomic schemes for the 21st century (Busschaert et al., 2022; Hanasaki et al., 2013; Wada et al., 2013). These
518   conclusions, however, only partially agree with the results of Khan et al. (2023), which show a decrease of irrigation at global

519 scale for scenario SSP5-8.5. This divergence is partly due to a decreasing trend in irrigated areas worldwide in Khan et al.
520 (2023), which is opposite to the positive trend prescribed by LUHv2. Results from Khan et al. (2023) rely on an integrated
521 assessment model, GCAM (Graham et al., 2020) which focuses on the integration of various socio-economic processes and
522 assumptions, with a prescribed, non-interactive, future climate scenario. Estimates of irrigated fractions within GCAM are
523 based on lumped values of water supply and water demand at the coarse scale of large river basins (Chen et al., 2020), although
524 these terms usually display strong irrigation and water resources heterogeneities in the real world. This calls for two
525 perspectives: firstly, to explore the effect of varied scenarios of irrigated areas on irrigation withdrawal in climate models;
526 secondly, to explore the inclusion of some socio-economic factors that control the evolution of irrigation and could improve
527 the representation of irrigation in LSMs, but are currently missing.
528 Finally, our findings on the hydroclimatic limits of irrigation activities bring a new perspective to the question of irrigation
529 sustainability. Our conclusions largely match those of Mehta et al. (2024), despite a different methodology and period of work.
530 Based on observed historical datasets, Mehta et al. (2024) show that many blue water-stressed regions exhibit an unsustainable
531 increase of irrigated areas in the early 21st century Based on a long-term simulation that considers changes in hydroclimatic
532 conditions and changes in irrigated areas, we also identify areas that could undergo unsustainable irrigation water withdrawals
533 at the end of the 21st century due to changes in the blue-water stress. Regions where our results differ from those of Mehta et
534 al. (2024) include irrigation hotspots such as the Mediterranean basin, southern South America, and Southeast Asia, which we
535 identify as areas of unsustainable irrigation in the future as a result of a more arid climate (e.g. the Iberian peninsula) or
536 overexploitation of water resources (e.g. southern South America and Southeast Asia). These results call to further explore the
537 sustainability of future irrigation scenarios within GHMs and LSMs, an important step for supporting the design of adaptation
538 policies at the regional scale for the water–food nexus.

539 **5 Conclusions**

540 We explored the joint evolution of irrigation activities, the water cycle and water resources under the SSP5-RCP-8.5 climate
541 change scenario, a scenario that could be seen as the upper boundary of potential climate change impacts. Our results suggest
542 that climate change and irrigation expansion will continue increasing global irrigation withdrawal in the future. The spatial
543 distribution of irrigation change is heterogeneous and depends on regional changes in climate and irrigated areas. The
544 enhancement in ET induced by irrigation will increase in irrigated areas and over land in the future. ET will also increase in
545 non-irrigated areas near irrigated zones owing to an increase in precipitation, but the influence of irrigation remains similar
546 under historical and future climate. Irrigation increases precipitation (with local exceptions), and the influence of irrigation on
547 precipitation remains similar under historical and future climate as well.
548 Historical depletion of water resources by irrigation will continue in the future, but our simulations reveal no major effect of
549 irrigation on river discharge seasonality under historical and future climate. In irrigated areas, climate change increases average
550 water resources (surface and groundwater), but irrigation activities can modulate the speed of change. In some non-irrigated

551 areas near irrigated zones, the increase in precipitation due to irrigation increases water resources under historic and future
552 climate (for instance, the Sahelian band and Central Asia), but the average irrigation influence in areas with no irrigation
553 remains weak throughout the simulation period. Importantly, we identified the areas in our simulation where irrigation could
554 be limited by future hydroclimate conditions (red class in our results) and the areas where irrigation could increase tensions
555 over the use of water resources (orange class in our results), which represent roughly one-third of the total irrigated areas (the
556 Mediterranean basin, Australia, California, Southeast Asia). Conversely, we determined areas where irrigation activities could
557 intensify or even partially convert to rainfed systems.

558 Eventually, our results underline the importance of including irrigation in climate change projections. It allows us to assess the
559 influence of future irrigation on water resources. Also, it helps to understand the complex feedback loops between irrigation,
560 water resources and future climate at global and regional scale, which is crucial for supporting the design of adaptation policies
561 of the water-food nexus in intensively irrigated regions. We remark that the description of irrigation in LSMs within ESMs
562 presents large uncertainties related to its biophysical and socio-economic drivers. This calls for enhanced multi-model studies,
563 as initiated within the IRRMIP framework (Yao et al., 2024), but it also calls for an important interdisciplinary effort to produce
564 contrasted yet plausible scenarios of future irrigated areas and irrigation practices, ideally accounting for the feedback from
565 non-agricultural water demand.

566

Author contribution

AD, FC and PFAO designed the study, AD, PFAO and JG run the simulations; PFAO wrote the first draft. All the authors
contributed to interpreting the results, discussing the findings and improving the final version of the paper.

Code availability

The version of the ORCHIDEE LSM used for this study corresponds to tag 2.2, revision 7709 (Arboleda-Obando et al., 2023),
and is freely available from https://forge.ipsl.jussieu.fr/orchidee/log/branches/ORCHIDEE_2_2/ , It is provided under a
CeCILL-C license (French equivalent to the LGPL license).

Competing interests

The contact author has declared that none of the authors has any competing interests.

Acknowledgement

This work has received support from Belmont Forum, BLUEGEM project (grant no. ANR-21-SOIL-0001). The simulations
were done and stored using the IDRIS computational facility (Institut du Développement et des Ressources en Informatique
Scientifique, CNRS, France) on the supercomputer Jean Zay CSL, under the allocation 2022[AD010113599R1].

582 **References**

583 Al-Yaari, A., Ducharne, A., Cheruy, F., Crow, W. T., and Wigneron, J. P.: Satellite-based soil moisture provides missing link
584 between summertime precipitation and surface temperature biases in CMIP5 simulations over conterminous United States, Sci
585 Rep, 9, 1–12, https://doi.org/10.1038/s41598-018-38309-5, 2019.

586 Al-Yaari, A., Ducharne, A., Thiery, W., Cheruy, F., and Lawrence, D.: The Role of Irrigation Expansion on Historical Climate
587 Change: Insights From CMIP6, Earths Future, 10, 1–29, https://doi.org/10.1029/2022EF002859, 2022.

588 Arboleda Obando, P. F., Ducharne, A., Cheruy, F., Jost, A., Ghattas, J., Colin, J., and Nous, C.: Influence of Hillslope Flow
589 on Hydroclimatic Evolution Under Climate Change, Earths Future, 10, 1–24, https://doi.org/10.1029/2021EF002613, 2022.

590 Arboleda-Obando, P. F., Ducharne, A., Yin, Z., and Ciais, P.: Validation of a new global irrigation scheme in the ORCHIDEE
591 land surface model - Dataset, https://doi.org/10.5281/zenodo.8014430, 2023.

592 Arboleda-Obando, P. F., Ducharne, A., Yin, Z., and Ciais, P.: Validation of a new global irrigation scheme in the land surface
593 model ORCHIDEE v2.2, Geosci Model Dev, 17, 2141–2164, https://doi.org/10.5194/gmd-17-2141-2024, 2024.

594 Beaumet, J., Krinner, G., Déqué, M., Haarsma, R., and Li, L.: Assessing bias corrections of oceanic surface conditions for
595 atmospheric models, Geosci Model Dev, 12, 321–342, https://doi.org/10.5194/gmd-12-321-2019, 2019.

596 Boucher, O., Servonnat, J., Albright, A. L., Aumont, O., Balkanski, Y., Bastrikov, V., Bekki, S., Bonnet, R., Bony, S., Bopp,
597 L., Braconnot, P., Brockmann, P., Cadule, P., Caubel, A., Cheruy, F., Codron, F., Cozic, A., Cugnet, D., D'Andrea, F., Davini,
598 P., Lavergne, C., Denvil, S., Deshayes, J., Devilliers, M., Ducharne, A., Dufresne, J., Dupont, E., Éthé, C., Fairhead, L., Falletti,
599 L., Flavoni, S., Foujols, M., Gardoll, S., Gastineau, G., Ghattas, J., Grandpeix, J., Guenet, B., Guez, Lionel, E., Guilyardi, E.,
600 Guimberteau, M., Hauglustaine, D., Hourdin, F., Idelkadi, A., Joussaume, S., Kageyama, M., Khodri, M., Krinner, G., Lebas,
601 N., Levavasseur, G., Lévy, C., Li, L., Lott, F., Lurton, T., Luyssaert, S., Madec, G., Madeleine, J., Maignan, F., Marchand,
602 M., Marti, O., Mellul, L., Meurdesoif, Y., Mignot, J., Musat, I., Ottlé, C., Peylin, P., Planton, Y., Polcher, J., Rio, C., Rochetin,
603 N., Rousset, C., Sepulchre, P., Sima, A., Swingedouw, D., Thiéblemont, R., Traore, A. K., Vancoppenolle, M., Vial, J., Vialard,
604 J., Viovy, N., and Vuichard, N.: Presentation and Evaluation of the IPSL-CM6A-LR Climate Model, J Adv Model Earth Syst,
605 12, 1–52, https://doi.org/10.1029/2019MS002010, 2020.

606 Busschaert, L., De Roos, S., Thiery, W., Raes, D., and De Lannoy, G. J. M.: Net irrigation requirement under different climate
607 scenarios using AquaCrop over Europe, Hydrol Earth Syst Sci, 26, 3731–3752, https://doi.org/10.5194/hess-26-3731-2022,
608 2022.

609 Chen, M., Vernon, C. R., Graham, N. T., Hejazi, M., Huang, M., Cheng, Y., and Calvin, K.: Global land use for 2015–2100
610 at 0.05° resolution under diverse socioeconomic and climate scenarios, Sci Data, 7, 320, https://doi.org/10.1038/s41597-020-
611 00669-x, 2020.

612 Cheruy, F., Ducharne, A., Hourdin, F., Musat, I., Vignon, É., Gastineau, G., Bastrikov, V., Vuichard, N., Diallo, B., Dufresne,
613 J., Ghattas, J., Grandpeix, J., Idelkadi, A., Mellul, L., Maignan, F., Ménégoz, M., Ottlé, C., Peylin, P., Servonnat, J., Wang, F.,

and Zhao, Y.: Improved Near-Surface Continental Climate in IPSL-CM6A-LR by Combined Evolutions of Atmospheric and

Land Surface Physics, J Adv Model Earth Syst, 12, https://doi.org/10.1029/2019MS002005, 2020.

Cook, B. I., Shukla, S. P., Puma, M. J., and Nazarenko, L. S.: Irrigation as an historical climate forcing, Clim Dyn, 44, 1715–

1730, https://doi.org/10.1007/s00382-014-2204-7, 2015.

Cook, B. I., McDermid, S. S., Puma, M. J., Williams, A. P., Seager, R., Kelley, M., Nazarenko, L., and Aleinov, I.: Divergent

Regional Climate Consequences of Maintaining Current Irrigation Rates in the 21st Century, Journal of Geophysical Research:

Atmospheres, 125, 1–22, https://doi.org/10.1029/2019JD031814, 2020.

Döll, P., Hoffmann-Dobrev, H., Portmann, F. T., Siebert, S., Eicker, A., Rodell, M., Strassberg, G., and Scanlon, B. R.: Impact

of water withdrawals from groundwater and surface water on continental water storage variations, J Geodyn, 59–60, 143–156,

https://doi.org/10.1016/j.jog.2011.05.001, 2012.

D'Orgeval, T., Polcher, J., and Rosnay, P. De: Sensitivity of the West African hydrological cycle in ORCHIDEE to infiltration

processes, Hydrol. Earth Syst. Sci., 12, 1387–1401, 2008.

Druel, A., Munier, S., Mucia, A., Albergel, C., and Calvet, J.-C.: Implementation of a new crop phenology and irrigation

scheme in the ISBA land surface model using SURFEX_v8.1, Geosci Model Dev, 15, 8453–8471,

https://doi.org/10.5194/gmd-15-8453-2022, 2022.

Frenken, K. and Gillet, V.: Irrigation water requirement and water withdrawal by country, Food and Agriculture Organization,

Rome, 265 pp., 2012.

Grafton, R. Q., Williams, J., and Jiang, Q.: Possible pathways and tensions in the food and water nexus, Earths Future, 5, 449–

462, https://doi.org/10.1002/2016EF000506, 2017.

Graham, N. T., Hejazi, M. I., Chen, M., Davies, E. G. R., Edmonds, J. A., Kim, S. H., Turner, S. W. D., Li, X., Vernon, C. R.,

Calvin, K., Miralles-Wilhelm, F., Clarke, L., Kyle, P., Link, R., Patel, P., Snyder, A. C., and Wise, M. A.: Humans drive future

water scarcity changes across all Shared Socioeconomic Pathways, Environmental Research Letters, 15, 014007,

https://doi.org/10.1088/1748-9326/ab639b, 2020.

Guimberteau, M., Drapeau, G., Ronchail, J., Sultan, B., Polcher, J., Martinez, J.-M., Prigent, C., Guyot, J.-L., Cochonneau,

G., Espinoza, J. C., Filizola, N., Fraizy, P., Lavado, W., De Oliveira, E., Pombosa, R., Noriega, L., and Vauchel, P.: Discharge

simulation in the sub-basins of the Amazon using ORCHIDEE forced by new datasets, Hydrol Earth Syst Sci, 16, 911–935,

https://doi.org/10.5194/hess-16-911-2012, 2012a.

Guimberteau, M., Laval, K., Perrier, A., and Polcher, J.: Global effect of irrigation and its impact on the onset of the Indian

summer monsoon, Clim Dyn, 39, 1329–1348, https://doi.org/10.1007/s00382-011-1252-5, 2012b.

Hanasaki, N., Fujimori, S., Yamamoto, T., Yoshikawa, S., Masaki, Y., Hijioka, Y., Kainuma, M., Kanamori, Y., Masui, T.,

Takahashi, K., and Kanae, S.: A global water scarcity assessment under Shared Socio-economic Pathways – Part 2: Water

availability and scarcity, Hydrol Earth Syst Sci, 17, 2393–2413, https://doi.org/10.5194/hess-17-2393-2013, 2013.

Hourdin, F., Rio, C., Grandpeix, J. Y., Madeleine, J. B., Cheruy, F., Rochetin, N., Jam, A., Musat, I., Idelkadi, A., Fairhead,

L., Foujols, M. A., Mellul, L., Traore, A. K., Dufresne, J. L., Boucher, O., Lefebvre, M. P., Millour, E., Vignon, E., Jouhaud,

648   J., Diallo, F. B., Lott, F., Gastineau, G., Caubel, A., Meurdesoif, Y., and Ghattas, J.: LMDZ6A: The Atmospheric Component
649   of the IPSL Climate Model With Improved and Better Tuned Physics, J Adv Model Earth Syst, 12, 1–37,
650   https://doi.org/10.1029/2019MS001892, 2020.

651   Hurtt, G. C., Chini, L., Sahajpal, R., Frolking, S., Bodirsky, B. L., Calvin, K., Doelman, J. C., Fisk, J., Fujimori, S., Klein
652   Goldewijk, K., Hasegawa, T., Havlik, P., Heinimann, A., Humpenöder, F., Jungclaus, J., Kaplan, J. O., Kennedy, J., Krisztin,
653   T., Lawrence, D., Lawrence, P., Ma, L., Mertz, O., Pongratz, J., Popp, A., Poulter, B., Riahi, K., Shevliakova, E., Stehfest, E.,
654   Thornton, P., Tubiello, F. N., van Vuuren, D. P., and Zhang, X.: Harmonization of global land use change and management
655   for the period 850–2100 (LUH2) for CMIP6, Geosci Model Dev, 13, 5425–5464, https://doi.org/10.5194/gmd-13-5425-2020,
656   2020.

657   IPCC: Climate Change 2021: The Physical Science Basis. Contribution of working group I to the Sixth Assessment Report of
658   the Intergovernmental Panel on Climate Change, edited by: Masson-Delmotte, V., Zhai, P., Pirani, A., Connors, S. L., Péan,
659   C., Berger, S., Caud, N., Chen, Y., Goldfarb, L., Gomis, M. I., Huang, M., Leitzell, K., Lonnoy, E., Matthews, J. B. R.,
660   Maycock, T. K., Waterfield, T., Yelekçi, O., Yu, R., and Zhou, B., Cambridge, UK and New York, USA, 2391 pp.,
661   https://doi.org/10.1017/9781009157896, 2021.

662   Khan, Z., Thompson, I., Vernon, C. R., Graham, N. T., Wild, T. B., and Chen, M.: Global monthly sectoral water use for
663   2010–2100 at 0.5° resolution across alternative futures, Sci Data, 10, 201, https://doi.org/10.1038/s41597-023-02086-2, 2023.

664   King, J. C., Connolley, W. M., and Derbyshire, S. H.: Sensitivity of modelled Antarctic climate to surface and boundary-layer
665   flux parametrizations, Quarterly Journal of the Royal Meteorological Society, 127, 779–794,
666   https://doi.org/10.1002/qj.49712757304, 2001.

667   Koster, R. D., Sud, Y. C., Guo, Z., Dirmeyer, P. A., Bonan, G., Oleson, K. W., Chan, E., Verseghy, D., Cox, P., Davies, H.,
668   Kowalczyk, E., Gordon, C. T., Kanae, S., Lawrence, D., Liu, P., Mocko, D., Lu, C.-H., Mitchell, K., Malyshev, S., McAvaney,
669   B., Oki, T., Yamada, T., Pitman, A., Taylor, C. M., Vasic, R., and Xue, Y.: GLACE: The Global Land–Atmosphere Coupling
670   Experiment. Part I: Overview, J Hydrometeorol, 7, 590–610, https://doi.org/10.1175/JHM510.1, 2006.

671   Krakauer, N. Y., Puma, M. J., Cook, B. I., Gentine, P., and Nazarenko, L.: Ocean–atmosphere interactions modulate
672   irrigation's climate impacts, Earth System Dynamics, 7, 863–876, https://doi.org/10.5194/esd-7-863-2016, 2016.

673   Krinner, G., Viovy, N., de Noblet-Ducoudré, N., Ogée, J., Polcher, J., Friedlingstein, P., Ciais, P., Sitch, S., and Prentice, I.
674   C.: A dynamic global vegetation model for studies of the coupled atmosphere-biosphere system, Global Biogeochem Cycles,
675   19, 1–33, https://doi.org/10.1029/2003GB002199, 2005.

676   Leng, G., Huang, M., Tang, Q., Sacks, W. J., Lei, H., and Leung, L. R.: Modeling the effects of irrigation on land surface
677   fluxes and states over the conterminous United States: Sensitivity to input data and model parameters, Journal of Geophysical
678   Research: Atmospheres, 118, 9789–9803, https://doi.org/10.1002/jgrd.50792, 2013.

679   Lepore, C., Abernathey, R., Henderson, N., Allen, J. T., and Tippett, M. K.: Future Global Convective Environments in CMIP6
680   Models, Earths Future, 9, 1–21, https://doi.org/10.1029/2021EF002277, 2021.

681 Lo, M.-H. and Famiglietti, J. S.: Irrigation in California's Central Valley strengthens the southwestern U.S. water cycle,
682 Geophys Res Lett, 40, 301–306, https://doi.org/10.1002/grl.50108, 2013.

683 Louis, J. F., Tiedtke, M., and Geleyn, J. F.: A Short History of the Operational PBL - Parameterization at ECMWF, 1982.

684 Lunel, T., Boone, A. A., and Le Moigne, P.: Irrigation strongly influences near-surface conditions and induces breeze
685 circulation: Observational and model-based evidence, Quarterly Journal of the Royal Meteorological Society, 150, 2798–2819,
686 https://doi.org/10.1002/qj.4736, 2024.

687 McDermid, S., Nocco, M., Lawston-Parker, P., Keune, J., Pokhrel, Y., Jain, M., Jägermeyr, J., Brocca, L., Massari, C., Jones,
688 A. D., Vahmani, P., Thiery, W., Yao, Y., Bell, A., Chen, L., Dorigo, W., Hanasaki, N., Jasechko, S., Lo, M.-H., Mahmood,
689 R., Mishra, V., Mueller, N. D., Niyogi, D., Rabin, S. S., Sloat, L., Wada, Y., Zappa, L., Chen, F., Cook, B. I., Kim, H.,
690 Lombardozzi, D., Polcher, J., Ryu, D., Santanello, J., Satoh, Y., Seneviratne, S., Singh, D., and Yokohata, T.: Irrigation in the
691 Earth system, Nat Rev Earth Environ, 4, 435–453, https://doi.org/10.1038/s43017-023-00438-5, 2023.

692 Mehta, P., Siebert, S., Kummu, M., Deng, Q., Ali, T., Marston, L., Xie, W., and Davis, K. F.: Half of twenty-first century
693 global irrigation expansion has been in water-stressed regions, Nature Water, 2, 254–261, https://doi.org/10.1038/s44221-024-
694 00206-9, 2024.

695 Ngo-Duc, T., Laval, K., Ramillien, G., Polcher, J., and Cazenave, A.: Validation of the land water storage simulated by
696 Organising Carbon and Hydrology in Dynamic Ecosystems (ORCHIDEE) with Gravity Recovery and Climate Experiment
697 (GRACE) data, Water Resour Res, 43, https://doi.org/10.1029/2006WR004941, 2007.

698 Okada, M., Iizumi, T., Sakamoto, T., Kotoku, M., Sakurai, G., Hijioka, Y., and Nishimori, M.: Varying Benefits of Irrigation
699 Expansion for Crop Production Under a Changing Climate and Competitive Water Use Among Crops, Earths Future, 6, 1207–
700 1220, https://doi.org/10.1029/2017EF000763, 2018.

701 Oki, T., Nishimura, T., and Dirmeyer, P.: Assessment of Annual Runoff from Land Surface Models Using Total Runoff
702 Integrating Pathways (TRIP), Journal of the Meteorological Society of Japan. Ser. II, 77, 235–255,
703 https://doi.org/10.2151/jmsj1965.77.1B_235, 1999.

704 Petit, O., Kuper, M., López-Gunn, E., Rinaudo, J., Daoudi, A., and Lejars, C.: Can agricultural groundwater economies
705 collapse? An inquiry into the pathways of four groundwater economies under threat, Hydrogeol J, 25, 1549–1564,
706 https://doi.org/10.1007/s10040-017-1567-3, 2017.

707 Pokhrel, Y., Hanasaki, N., Koirala, S., Cho, J., Yeh, P. J. F., Kim, H., Kanae, S., and Oki, T.: Incorporating Anthropogenic
708 Water Regulation Modules into a Land Surface Model, J Hydrometeorol, 13, 255–269, https://doi.org/10.1175/JHM-D-11-
709 013.1, 2012.

710 Pokhrel, Y. N., Koirala, S., Yeh, P. J.-F., Hanasaki, N., Longuevergne, L., Kanae, S., and Oki, T.: Incorporation of groundwater
711 pumping in a global Land Surface Model with the representation of human impacts, Water Resour Res, 51, 78–96,
712 https://doi.org/10.1002/2014WR015602, 2015.

713 Pokhrel, Y. N., Hanasaki, N., Wada, Y., and Kim, H.: Recent progresses in incorporating human land-water management into
714 global land surface models toward their integration into Earth system models, Wiley Interdisciplinary Reviews: Water, 3, 548–
715 574, https://doi.org/10.1002/wat2.1150, 2016.

716 Qiao, L., Zuo, Z., Zhang, R., Piao, S., Xiao, D., and Zhang, K.: Soil moisture–atmosphere coupling accelerates global warming,
717 Nat Commun, 14, 4908, https://doi.org/10.1038/s41467-023-40641-y, 2023.

718 Risi, C., Noone, D., Frankenberg, C., and Worden, J.: Role of continental recycling in intraseasonal variations of continental
719 moisture as deduced from model simulations and water vapor isotopic measurements, Water Resour Res, 49, 4136–4156,
720 https://doi.org/10.1002/wrcr.20312, 2013.

721 de Rosnay, P., Polcher, J., Laval, K., and Sabre, M.: Integrated parameterization of irrigation in the land surface model
722 ORCHIDEE. Validation over Indian Peninsula, Geophys Res Lett, 30, 1986, https://doi.org/10.1029/2003GL018024, 2003.

723 Sadourny, R. and Laval, K.: January and July performance of the LMD general circulation model, in: New Perspectives in
724 Climate Modelling, edited by: Berger, A. and Nicolis, C., Elsevier, Amsterdam, 173–197, 1984.

725 Schwarzwald, K. and Lenssen, N.: The importance of internal climate variability in climate impact projections, Proceedings
726 of the National Academy of Sciences, 119, https://doi.org/10.1073/pnas.2208095119, 2022.

727 Seneviratne, S. I., Wilhelm, M., Stanelle, T., Van Den Hurk, B., Hagemann, S., Berg, A., Cheruy, F., Higgins, M. E., Meier,
728 A., Brovkin, V., Claussen, M., Ducharne, A., Dufresne, J. L., Findell, K. L., Ghattas, J., Lawrence, D. M., Malyshev, S.,
729 Rummukainen, M., and Smith, B.: Impact of soil moisture-climate feedbacks on CMIP5 projections: First results from the
730 GLACE-CMIP5 experiment, Geophys Res Lett, 40, 5212–5217, https://doi.org/10.1002/grl.50956, 2013.

731 Siebert, S. and Döll, P.: Quantifying blue and green virtual water contents in global crop production as well as potential
732 production losses without irrigation, J Hydrol (Amst), 384, 198–217, https://doi.org/10.1016/j.jhydrol.2009.07.031, 2010.

733 Siebert, S., Burke, J., Faures, J. M., Frenken, K., Hoogeveen, J., Döll, P., and Portmann, F. T.: Groundwater use for irrigation
734 - A global inventory, Hydrol Earth Syst Sci, 14, 1863–1880, https://doi.org/10.5194/hess-14-1863-2010, 2010.

735 Siebert, S., Kummu, M., Porkka, M., Döll, P., Ramankutty, N., and Scanlon, B. R.: A global data set of the extent of irrigated
736 land from 1900 to 2005, Hydrol Earth Syst Sci, 19, 1521–1545, https://doi.org/10.5194/hess-19-1521-2015, 2015.

737 Tafasca, S., Ducharne, A., and Valentin, C.: Weak sensitivity of the terrestrial water budget to global soil texture maps in the
738 ORCHIDEE land surface model, Hydrol Earth Syst Sci, 24, 3753–3774, https://doi.org/10.5194/hess-24-3753-2020, 2020.

739 Taranu, S. I., Lawrence, D. M., Wada, Y., Tang, T., Kluzek, E., Rabin, S., Yao, Y., De Hertog, S. J., Vanderkelen, I., and
740 Thiery, W.: Bridging the gap: a new module for human water use in the Community Earth System Model version 2.2.1, Geosci
741 Model Dev, 17, 7365–7399, https://doi.org/10.5194/gmd-17-7365-2024, 2024.

742 Taylor, R. G., Scanlon, B., Döll, P., Rodell, M., van Beek, R., Wada, Y., Longuevergne, L., Leblanc, M., Famiglietti, J. S.,
743 Edmunds, M., Konikow, L., Green, T. R., Chen, J., Taniguchi, M., Bierkens, M. F. P., MacDonald, A., Fan, Y., Maxwell, R.
744 M., Yechieli, Y., Gurdak, J. J., Allen, D. M., Shamsudduha, M., Hiscock, K., Yeh, P. J. F., Holman, I., and Treidel, H.: Ground
745 water and climate change, Nat Clim Chang, 3, 322–329, https://doi.org/10.1038/nclimate1744, 2013.

Tebaldi, C., Debeire, K., Eyring, V., Fischer, E., Fyfe, J., Friedlingstein, P., Knutti, R., Lowe, J., O'Neill, B., Sanderson, B., Van Vuuren, D., Riahi, K., Meinshausen, M., Nicholls, Z., Tokarska, K., Hurtt, G., Kriegler, E., Meehl, G., Moss, R., Bauer, S., Boucher, O., Brovkin, V., Yhb, Y., Dix, M., Gualdi, S., Guo, H., John, J., Kharin, S., Kim, Y. H., Koshiro, T., Ma, L., Olivié, D., Panickal, S., Qiao, F., Rong, X., Rosenbloom, N., Schupfner, M., Séférian, R., Sellar, A., Semmler, T., Shi, X., Song, Z., Steger, C., Stouffer, R., Swart, N., Tachiiri, K., Tang, Q., Tatebe, H., Voldoire, A., Volodin, E., Wyser, K., Xin, X., Yang, S., Yu, Y., and Ziehn, T.: Climate model projections from the Scenario Model Intercomparison Project (ScenarioMIP) of CMIP6, Earth System Dynamics, 12, 253–293, https://doi.org/10.5194/esd-12-253-2021, 2021.

Thiery, W., Visser, A. J., Fischer, E. M., Hauser, M., Hirsch, A. L., Lawrence, D. M., Lejeune, Q., Davin, E. L., and Seneviratne, S. I.: Warming of hot extremes alleviated by expanding irrigation, Nat Commun, 11, 1–7, https://doi.org/10.1038/s41467-019-14075-4, 2020.

Vicente-Serrano, S. M., Peña-Gallardo, M., Hannaford, J., Murphy, C., Lorenzo-Lacruz, J., Dominguez-Castro, F., López-Moreno, J. I., Beguería, S., Noguera, I., Harrigan, S., and Vidal, J. -P.: Climate, Irrigation, and Land Cover Change Explain Streamflow Trends in Countries Bordering the Northeast Atlantic, Geophys Res Lett, 46, 10821–10833, https://doi.org/10.1029/2019GL084084, 2019.

Vignon, E., Hourdin, F., Genthon, C., Gallée, H., Bazile, E., Lefebvre, M., Madeleine, J., and Van de Wiel, B. J. H.: Antarctic boundary layer parametrization in a general circulation model: 1-D simulations facing summer observations at Dome C, Journal of Geophysical Research: Atmospheres, 122, 6818–6843, https://doi.org/10.1002/2017JD026802, 2017.

Vörösmarty, C. J., Fekete, B. M., Meybeck, M., and Lammers, R. B.: Global system of rivers: Its role in organizing continental land mass and defining land-to-ocean linkages, Global Biogeochem Cycles, 14, 599–621, https://doi.org/10.1029/1999GB900092, 2000.

de Vrese, P. and Hagemann, S.: Uncertainties in modelling the climate impact of irrigation, Clim Dyn, 51, 2023–2038, https://doi.org/10.1007/s00382-017-3996-z, 2018.

de Vrese, P., Hagemann, S., and Claussen, M.: Asian irrigation, African rain: Remote impacts of irrigation, Geophys Res Lett, 43, 3737–3745, https://doi.org/10.1002/2016GL068146, 2016a.

de Vrese, P., Schulz, J.-P., and Hagemann, S.: On the Representation of Heterogeneity in Land-Surface–Atmosphere Coupling, Boundary Layer Meteorol, 160, 157–183, https://doi.org/10.1007/s10546-016-0133-1, 2016b.

Wada, Y., Wisser, D., Eisner, S., Flörke, M., Gerten, D., Haddeland, I., Hanasaki, N., Masaki, Y., Portmann, F. T., Stacke, T., Tessler, Z., and Schewe, J.: Multimodel projections and uncertainties of irrigation water demand under climate change, Geophys Res Lett, 40, 4626–4632, https://doi.org/10.1002/grl.50686, 2013.

Wei, J., Dirmeyer, P. A., Wisser, D., Bosilovich, M. G., and Mocko, D. M.: Where does the irrigation water go? An estimate of the contribution of irrigation to precipitation using MERRA, J Hydrometeorol, 14, 275–289, https://doi.org/10.1175/JHM-D-12-079.1, 2013.

Wild, M.: The global energy balance as represented in CMIP6 climate models, Clim Dyn, 55, 553–577, https://doi.org/10.1007/s00382-020-05282-7, 2020.

780 Yao, Y., Vanderkelen, I., Lombardozzi, D., Swenson, S., Lawrence, D., Jägermeyr, J., Grant, L., and Thiery, W.:
781 Implementation and Evaluation of Irrigation Techniques in the Community Land Model, J Adv Model Earth Syst, 14, 1–27,
782 https://doi.org/10.1029/2022MS003074, 2022.

783 Yao, Y., Ducharne, A., Cook, B. I., Hertog, S. J. De, Aas, K. S., Arboleda-Obando, P. F., Buzan, J., Colin, J., Costantini, M.,
784 Decharme, B., Lawrence, D. M., Peter5Lawrence, Leung, L. R., Lo, M.-H., Narayanappa, D., Wieder, W., Wu, R.-J., Zhou,
785 T., Jägermeyr, J., McDermid, S., Pokhrel, Y., Elling, M., Hanasaki, N., Muñoz, P., Nazarenko, L., Otta, K., Satoh, Y.,
786 Yokohata, T., Jin, L., Wang, X., Mishra, V., Ghosh, S., and Thiery, W.: Impacts of irrigation expansion on moist-heat stress:
787 first results from IRRMIP, PREPRINT (Version 1) available at Research Square,
788 https://doi.org/https://doi.org/10.21203/rs.3.rs-4835411/v1, 2024.

789 Yin, Z., Wang, X. H., Ottlé, C., Zhou, F., Guimberteau, M., Polcher, J., Peng, S. S., Piao, S. L., Li, L., Bo, Y., Chen, X. L.,
790 Zhou, X. D., Kim, H., and Ciais, P.: Improvement of the Irrigation Scheme in the ORCHIDEE Land Surface Model and
791 Impacts of Irrigation on Regional Water Budgets Over China, J Adv Model Earth Syst, 12, 1–20,
792 https://doi.org/10.1029/2019MS001770, 2020.

793 Zhou, S., Williams, A. P., Lintner, B. R., Berg, A. M., Zhang, Y., Keenan, T. F., Cook, B. I., Hagemann, S., Seneviratne, S.
794 I., and Gentine, P.: Soil moisture–atmosphere feedbacks mitigate declining water availability in drylands, Nat Clim Chang,
795 11, 38–44, https://doi.org/10.1038/s41558-020-00945-z, 2021.

796 Zobler, L.: A world soil hydrology file for global climate modeling, Technical Memorandum 87802, National Aeronautics and
797 Space Administration, 1986.

798
799